HYDROTHERMAL ALTERATION OF OCEANIC LITHOSPHERE: A GEOCHEMICAL STUDY OF THE OMAN OPHIOLITE

A Thesis
Presented to the Faculty of the Graduate School
of Cornell University
in Partial Fulfillment of the Requirements for the Degree of
Master of Science

By
Chen Chen
January 2012

HYDROTHERMAL ALTERATION OF OCEANIC LITHOSPHERE: A GEOCHEMICAL STUDY OF THE OMAN OPHIOLITE

Chen Chen

Cornell University 2012

The Oman ophiolite, one of the best preserved and best exposed ophiolites, is part of the Tethyan Ophiolite series in the Mediterranean, formed during the spreading of Tethys Ocean and obducted during the closure of this ocean. Isotopic, major and trace element analyses were conducted on samples collected from Nahkl, Sumail and Wadi-Tayin nappes in this study. $^{87}Sr/^{86}Sr$ and $\delta^{18}O$ values indicate the circulation system is not a decoupled two-layer alteration system. Instead, high temperature alteration and low temperature alteration are alternately swiping down to the lower gabbro section, as suggested by Nicolas *et al* 2003. Fixation of CO_2 into ultramafic rocks after the obduction has changed the isotopic compositions, increasing the $^{87}Sr/^{86}Sr$ and $\delta^{18}O$ values, which should be considered when interpreting isotope ratios of ophiolites.

BIOGRAPHIC SKETCH

Chen Chen was born in Xinyang, Henan Province, China, but grew up in Qingdao, Shandong Province. She had a wonderful childhood in the coastal city and her memories were full of delicious seafood and happy times at the beach. In high school, she studied very hard in order to be admitted to a good university, as all Chinese students do. She originally chose Civil Engineering as first undergraduate major and English as second, however was assigned to the field of Geochemistry. At China University of Geosciences (Wuhan), she found out that Earth Science is actually very different from simply coal mining, and studying the Earth is a very fascinating subject. After four years of classroom lectures and summer field schools, she decided to continue her interest in exploring the Earth in the United States. Since summer 2008, she has been studying with Professor William White at Cornell University. Life at graduate school, though challenging, has been an exciting and rewarding experience. She has learned how to cope with difficulties that life throws up, and is now ready to turn over a new page in her life.

BIOGRAPHIC SKETCH

Chen Chen was born in Xinyang, Henan Province, China, but grew up in Qingdao, Shandong Province. She had a wonderful childhood in the coastal city and her memories were full of delicious seafood and happy times at the beach. In high school, she studied very hard in order to be admitted to a good university, as all Chinese students do. She originally chose Civil Engineering as first undergraduate major and English as second, however was assigned to the field of Geochemistry. At China University of Geosciences (Wuhan), she found out that Earth Science is actually very different from simply coal mining, and studying the Earth is a very fascinating subject. After four years of classroom lectures and summer field schools, she decided to continue her interest in exploring the Earth in the United States. Since summer 2008, she has been studying with Professor William White at Cornell University. Life at graduate school, though challenging, has been an exciting and rewarding experience. She has learned how to cope with difficulties that life throws up, and is now ready to turn over a new page in her life.

ACKNOWLEDGMENTS

I would like to firstly thank my advisors Professor William White and Professor Christopher Andronicos for their generous support and guidance that I am truly thankful for. It has been a great pleasure to work with them, critically discuss results and get helpful guidance on research from them. They not only taught me a serious attitude towards research is very important, but also gave me advice on life choices. Professor Louis Derry helped me a lot with laboratory work and data processing. Both his intelligence and humor really made problems much easier to solve. Professor Lawrence Cathles has supported the field trips and the chemistry analyses in this study. Without his help, the study would not have been able to happen.

I would also like to thank my fellow students Naomi Kirk-Lawlor, Kyle Trostle, Sander Hunter, Herdis Schopka, Ceren Karaca, Phoebe Judge, Gregg McElwee, Felipe Aron, Ashley Tibbetts, Caitlin Cox, Scott Henderson and many more who have helped me through difficulties in my studies and in my personal life. Having all of you as friends have made my graduate student life so enjoyable. I am greatly indebted to George Hade for his help with laboratory equipments. Without his help, I would not be able to get $^{87}Sr/^{86}Sr$ data, which is very important for this thesis. With the help of John Hunt, I have learned how to do microprobe work and conducted major element analysis.

Finally, I would like to thank my parents Yiyuan Chen and Ying Wang and my good friends Sally Tang, Ben Hasseldine, Shanshan Zhang for their unwavering support.

TABLE OF CONTENTS

LIST OF FIGURES

LIST OF TABLES

INTRODUCTION

Hydrothermal circulation occurring in oceanic crust impacts a variety of physical, chemical, and biological processes. Hydrothermal systems, known as black smokers because of their high concentration of minerals precipitating from the venting fluids, are found in the axial zone of ridge segments and have vent fluid temperatures up to 350 ~ 400 °C. The mineral-rich hot fluid cools quickly as it mixes with cold seawater, resulting in precipitation that creates chimney-like formations. Farther away from the ridge axis, the temperature of hydrothermal vents can be as low as 20°C. Globally, hydrothermal circulation systems are responsible for 20% of Earth's total heat loss, or about 11 TW [Stein and Stein, 1994]. The hydrothermal fluid interacts with oceanic crust that it passes through, exchanging elements and altering the composition of the oceanic crust. Subduction of altered oceanic lithosphere into mantle contributes to the chemical heterogeneity of the mantle and affects its rheology. As a result, it is important to understand the hydrothermal circulation process occurring in the oceanic lithosphere and to quantify the elemental exchange and chemical reactions.

The most direct way of studying the hydrothermal process is *in situ* oceanic crust analysis. However, the limited access and high expense of operating deep-ocean drilling and submersibles encourage us to find other methods to approach. Ophiolites, which are thought to represent a section of oceanic lithosphere, offers extensive exposure over large areas on land. For this reason, ophiolites are key to

understand the relationship between primary oceanic crust and hydrothermal processes.

The purpose of this study is to determine the depth and type of hydrothermal alteration in the Oman ophiolite section through analyses of strontium and oxygen isotope ratios and major and trace elements. The principal goals of the study were to determine the depth of hydrothermal circulation at the ridge crest and how much of the mantle peridotite had become serpentinized in the process. This study is important because the Oman ophiolite is thought to represent a slice of oceanic lithosphere formed at a spreading tectonic environment around 95 million years ago [Tilton *et al.*, 1981]. The studies of the ophiolite can shed light on the hydrothermal alteration happening at mid ocean ridge which is the most common extensional oceanic environment on the Earth. It is also meaningful to learn the chemical and mineralogical compositions of hydrothermally altered oceanic lithosphere. The mineralogy of the mantle affects its rheology, which plays an important role in the dynamics of lithosphere and asthenosphere. As CO_2 sequestration receives more attention, more researches are recently being done on ophiolites because the peridotite section is a potential permanent CO_2 storage reservoir [Seifritz, 1990; Lackner *et al.*, 1995; Kelemen and Matter, 2008].

Development of the Concept of Ophiolite

What is an ophiolite? In ancient Greek, 'ophio' means pertaining to snakes and 'lite' or more commonly 'litho' means rock. As a result, ophiolite means rocks that look like snakes. The green color and snake texture of the rocks come from the

interaction with ocean water. Nicolas (1989) gave an excellent review of the historical development of the ophiolite concept in the book "Structures of Ophiolites and Dynamics of Oceanic Lithosphere", and the following summary comes largely from that book.

Since Brongniart (1813) first defined ophiolite as serpentinites in mélanges in the Alps in 1813, the concept has gone through several phases of evolution. In 1821, Brongniart redefined the concept 'ophiolite' as a suite of magmatic rocks occurring in the Apennines. Subsequent studies of ophiolites were carried out by European geologists in the Apennines as well as the western Alps. The association of radiolarite, diabase, gabbro and peridotites was not identified until the beginning of 20th century. In 1927, Steinmann (1927) defined ophiolites as a group of spatially associated rocks that formed as in situ intrusions in geosynclines and emphasized the occurrence of peridotite, gabbro, diabase-spilite in association with deep-sea sedimentary rocks, in the Mediterranean mountain chains. The association of serpentinite, diabase-spilite and chert is known as 'Steinmann trinity'.

While the European geologists had already recorded the genetic association of peridotite, gabbro and basaltic rocks in the ophiolite assemblages in 1920's, there was debate over the interpretation of peridotites inside of the American camp. Benson (1926) interpreted the peridotites and serpentinites in mountain belts as plutonic intrusions of ultramafic magmas at crustal level. Bowen (1927) introduced a different interpretation of peridotites from his experimental results: because of the lack of ultramafic lavas, the peridotites and serpentinites formed from injections

of olivine- and pyroxene- rich masses in the solid state. The research that focused on the origin of peridotites and serpentinites as separate units from mafic rocks had set back the American geologists' understanding of the significance of the genetic link between plutonic-volcanic and ultramafic rocks in ophiolites [Dilek, 2003].

In 1950s and 1960s, several European geologists proposed a single magmatic origin of ophiolite suites: the crystallization of magma produced a stratigraphic order from peridotites at the bottom upwards into gabbros, with basaltic lavas on top [Dubertret, 1955; Brunn, 1956, 1960, 1961; Aubouin and Ndojaj, 1964]. However, Vuagnat (1963) pointed out the impossibility of balancing the small mafic section with the dominant peridotite section if both are formed by differentiation of basaltic magma. Vuagnat suggested that the peridotites in ophiolites were partial melting residues in the upper mantle. By 1960s, the structure of oceanic crust had been inferred from seismic studies [e.g., Ewing and Ewing, 1959]. Field observations of ophiolites in Italy and Cyprus led to the assumption of ophiolites as oceanic crust formed at a spreading center [Gass, 1968; Bezzi and Piccardo, 1971]. The introduction of plate tectonics theory in 1970s provided possible explanations for ophiolite-oceanic floor analogy.

The International Penrose Field Conference on ophiolites in September 1972 gathered European and American geologists, and produced a consensus statement on the definition of an ophiolite, more than 150 years after the first introduction of the concept (Anonymous, 1972). According to the definition agreed at the conference: "Ophiolite refers to a distinctive assemblage of mafic to ultramafic

rocks. It should not be used as a rock name or as a lithologic unit in mapping. In a completely developed ophiolite, the rock types occur in the following sequence, starting from the bottom and working up (Figure 1):

-Ultramafic complex, consisting of variable proportions of harzburgite, lherzolite and dunite, usually with a metamorphic tectonic fabric (more or less serpentinized);

-Gabbroic complex, ordinarily with cumulus textures commonly containing cumulus peridotites and pyroxenites and usually less deformed than the ultramafic complex;

-Mafic sheeted dike complex;

-Mafic volcanic complex, commonly pillowed.

-Associate rock types include (1) an overlying sedimentary section typically including ribbon cherts, thin shale interbeds, and minor limestones; (2) podiform bodies of chromite generally associated with dunite; and (3) sodic felsic intrusive and extrusive rocks.

Faulted contacts between mappable units are common. Whole sections may be missing. An ophiolite may be incomplete, dismembered, or metamorphosed ophiolite. Although ophiolite generally is interpreted to be oceanic crust and upper mantle, the use of the tern should be independent of its supposed origin".

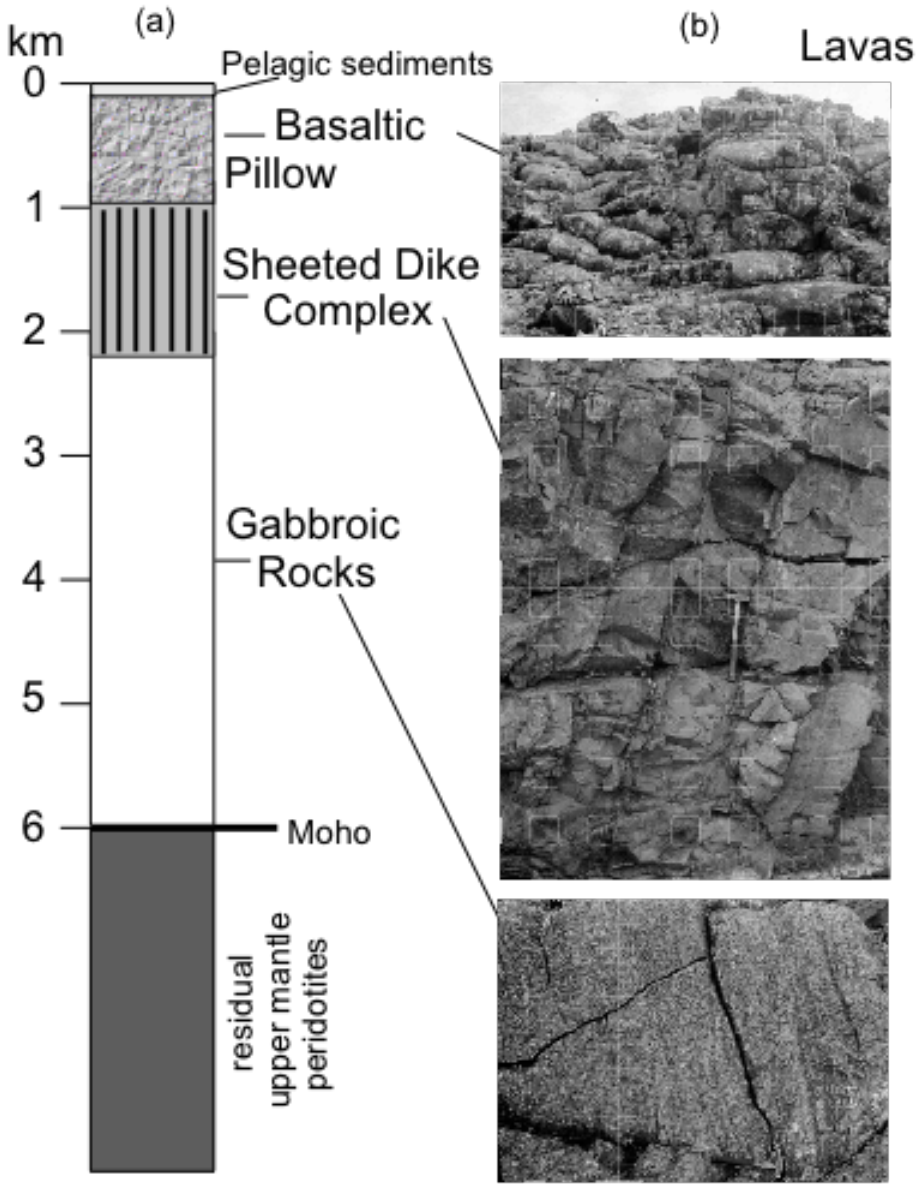

Figure 1. (a) Generalized internal structure and interpretation of the oceanic crust derived from studies of ophiolite complexes and interpretations of marine seismic and geologic data. (b) Outcrop photographs of crustal rocks from ophiolites; top: pillow lavas, Macquarie Island; middle: sheeted dike complex, Oman; bottom: gabbroic rocks, Bay of Islands. After Karson (2002).

Magmatic Process at Ocean Ridges

At ocean ridges, the seafloor spreading creates a 'gap' and asthenosphere rises to fill to it. However, the asthenosphere decompresses as it rises and consequently eventually crosses its solidus and melting begins to produce basaltic magma. The magma rises buoyantly until it reaches the Moho, where it stalls because it is no longer buoyant. Here it forms a magma chamber and undergoes fractional crystallization. Crystals produced in the process accumulate as layered gabbros at the bottom of magma chamber. Much of the magma, however, crystallizes in place forming the massive gabbros in the upper part of the lower crust. A small fraction, perhaps only 20%, of the remaining magma rises to the surface and erupts forming pillow lavas. The sheeted dikes begin as the conduits through which the magma rose to the surface. As the eruption ends, magma in the conduits freezes to form dikes. Above the pillow basalts, ocean sediments settle down through time.

An ideal ophiolite succession will have this complete sequence. Most ophiolites, however, are missing one or more of these units. The Oman ophiolite is one of the few that have a complete sequence. In addition to its completeness, the size of the Oman ophiolite (450 km long and 50~100 km wide), excellent exposure in a desert environment, and easy access in the field make it among the best examples for study.

Geological Setting of the Oman Ophiolite

The Oman ophiolite, also called the Semail ophiolite, is one of the best preserved and best exposed in the world. Most of the ophiolite is located in northern part of the Sultanate of Oman, with a small portion in United Arab Emirates (Figure 2). The ophiolite starts on the Musandam Peninsula (26°N, 56.3°E) and is elongate southeastward, extending to Ras Al Hadd, the most easterly point in Oman (22.517°N, 59.767°E). The length of the entire ophiolite is about 450km, and the width of each nappe ranges from 50 to 100km. The Oman Ophiolite is part of the Tethyan Ophiolite series in the Mediterranean region. The Tethyan Ophiolites were formed during the spreading of Tethys Ocean and obducted during the closure of this ocean [Coleman, 1981]. The ophiolite series was broken into massifs during their obduction. My samples were collected from the Nakhal, Sumail (a massif crosses by the Wadi Sumail), and Wadi-Tayin nappes (Figure 2).

The Oman Ophiolite represents a complete sequence of 5-7 km of oceanic crust underlain by 10 km of mantle peridotite and composed of, from the bottom to the top: mantle peridotite, the Moho transition zone (MTZ) or mantle-crust transition zone, layered gabbro, massive gabbro, sheeted dikes, pillow basalts and a layer of sediments [Boudier *et al*., 1988; Nicolas *et al*., 1988a]. The MTZ is a few to several hundred-meter thick, made of dunites.

Below the peridotite tectonites is a few hundred-meter thick metamorphic sole [Hacker, 1994]. The metamorphic sole formed during the obduction of the

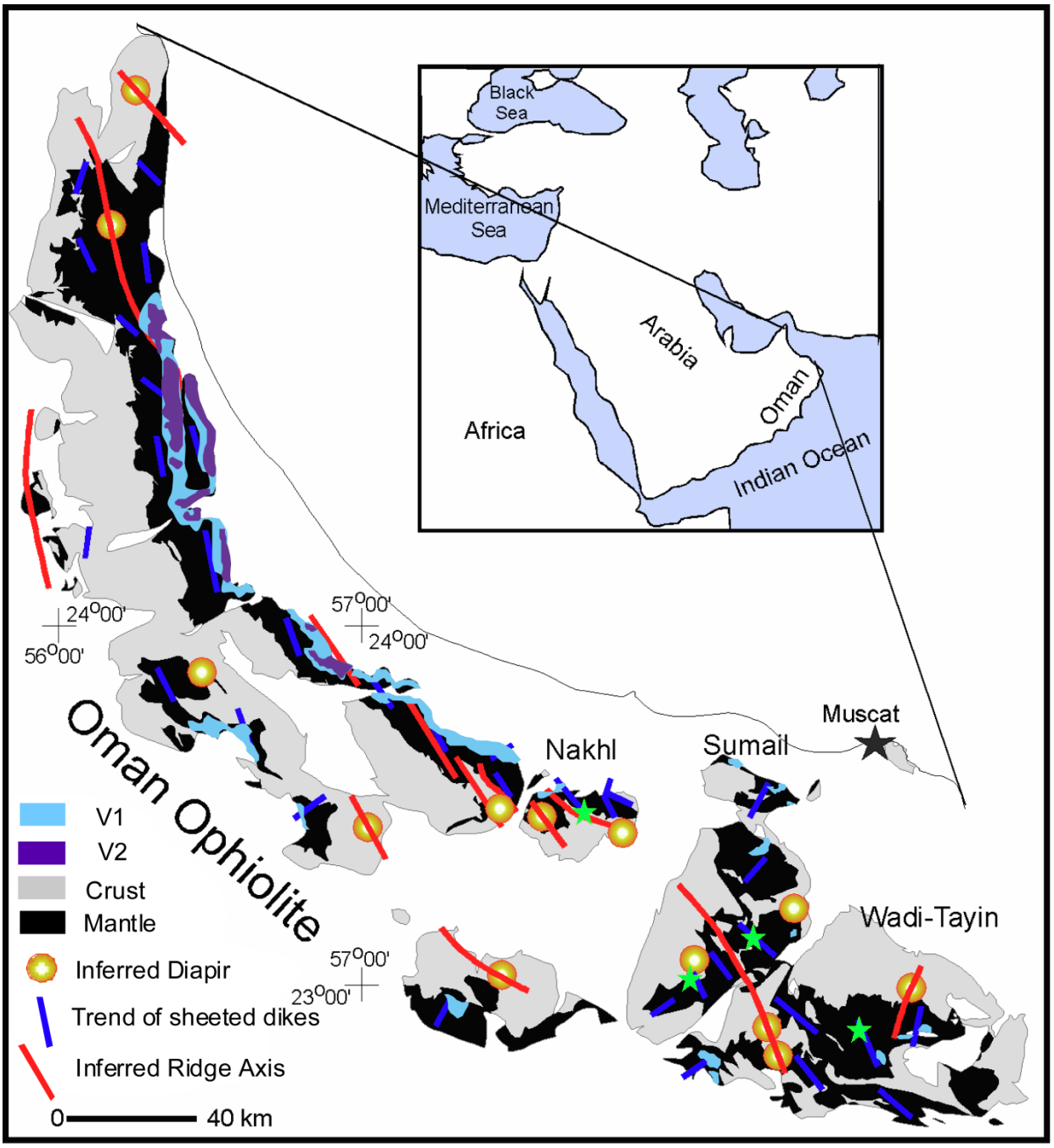

Figure 2. Simplified geologic map of the Oman ophiolite modified from Nicolas *et al.* (2000) depicting the crust (black), mantle (gray), lava series 1 (blue) and lava series 2 (purple). Trend of sheeted dikes (blue lines), inferred ridge axis (red lines) and inferred diapirs (orange circles) are shown. Nakhal, Sumail and Wadi-Tayin nappes where samples were collected are labeled. Green stars show sampling locations. Inset shows location of the Oman ophiolite.

oceanic lithosphere. At Wadi Tayin, this sole underlies tectonized harzburgite and consists of garnet amphibolite grading downward into garnet-free amphibolite, greenschist and metasedimentary and metavolcanic rocks [Searle and Malpas, 1980; Ghent and Stout, 1981; Hacker, 1994]. The garnet amphibolite records the highest temperature of 755-865°C and pressures of 200-500 MPa [Searle and Malpas, 1980; Ghent and Stout, 1981]. The $^{40}Ar/^{39}Ar$ dates of hornblende separates from the amphibolite have a mean age of 93.7 Ma, and the U/Pb zircon ages from the plagiogranites in the crustal section which represent the crystallization age of the crust have a mean value of 94.8 Ma [Tilton *et al*., 1981; Hacker, 1994]. The age difference between the metamorphic sole and the plagiogranites suggest that cooling of the oceanic lithosphere to <525°C occurred within ~1 million years of crystallization of the ophiolite [Hacker, 1994].

A few important geologic units in the area of the Oman ophiolite are (Figure 3): the Hajar Supergroup, a para-autochthonous set of middle Permian to middle Senonian continental-shelf carbonates; the allochthonous units, the Oman ophiolite which represents oceanic lithosphere and the Hawasina formation which is composed of Mid-Permian to Senonian continental slope and abyssal sediments and limestones; the autochthonous Maastrichtian to Miocene shallow water carbonates [Glennie *et al*., 1973; Coleman, 1981; Gray *et al*., 2000; Robertson, 2004].

Mid-Ocean Ridge vs. Supra-Subduction Zone

Although the first detailed study of the Oman ophiolite was made in 1960s, its tectonic setting is still controversial. Two theories prevail as to the tectonic

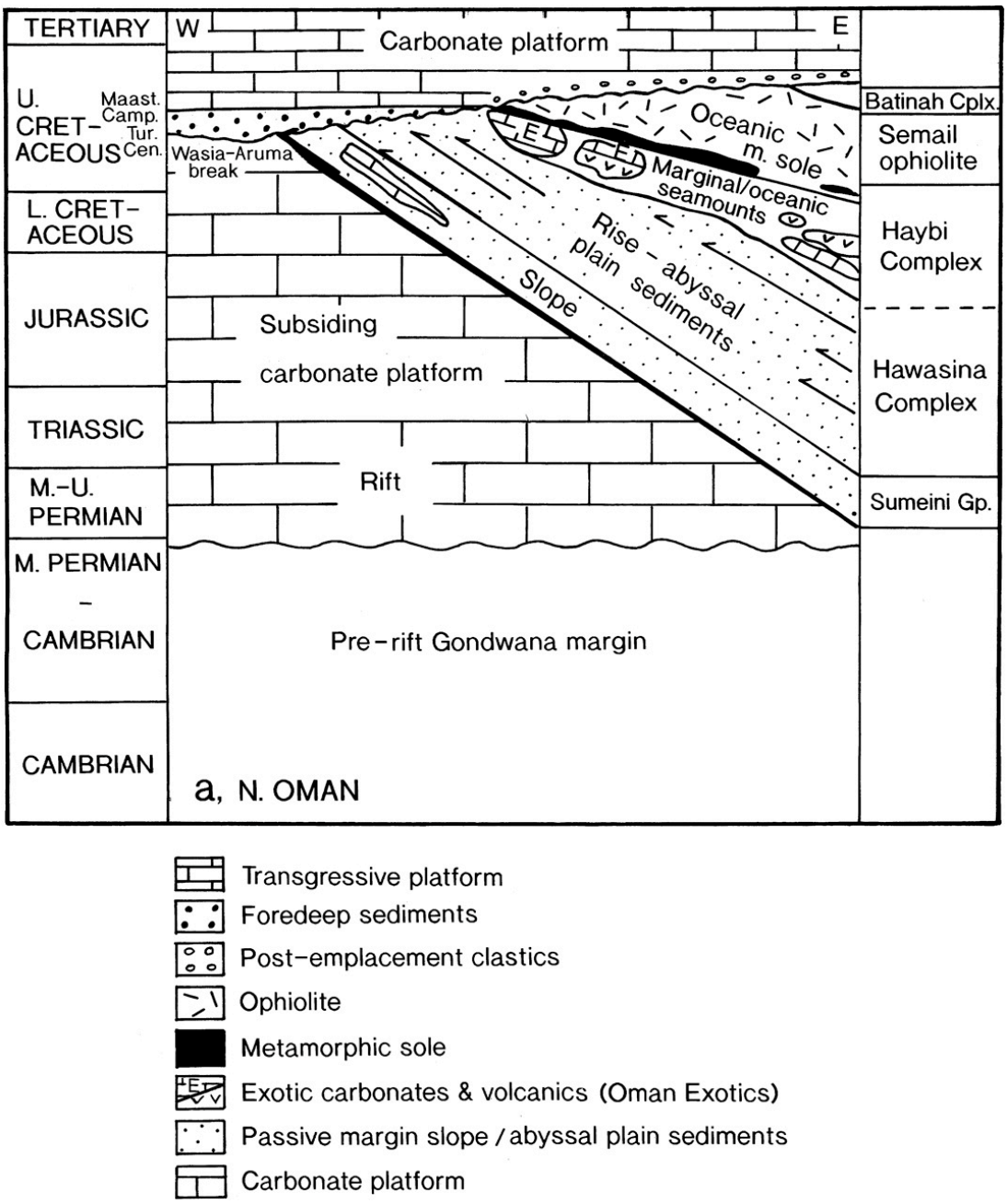

Figure 3. Simplified tectonostratigraphy showing the relation of the rifted margins sediments and volcanics (Hawasina Complex) beneath the Semail ophiolite, also the relative positions of the Haybi Complex and the Oman Exotics. From Robertson (2004); based on work done by Glennie *et al.* (1973).

setting in which the Oman ophiolite was formed: mid-ocean ridge (MOR) and supra-subduction zone (SSZ). SSZ ophiolites have the structure of oceanic lithosphere but island arc geochemical features [Pearce *et al.*, 1984]. Although subduction zones are areas of plate convergence and hence for the most part quite distinct from the mid-ocean ridges, spreading can and does often occur near island arc on the overlying or footwall plate. Modern examples include the Mariana and Bonin arcs [Tarney *et al.*, 1981; Hawkins and Mechior, 1985; Sinton and Fryer, 1987].

Glennie *et al.* (1973, 1974) reconstructed the Hawasina basin through stratigraphic and paleontological studies and concluded that it originated as part of a deep ocean bounded by the Arabian continental margin to the south and the Tethyan Sea spreading ridge to the northeast. The Semail Ophiolite obducted onto Hawasina sedimentary rocks, and that obduction placed the Semail and Hawasina Nappes above Arabian continental margin. The Semail and Hawasina Nappes were covered by a shallow sea until the end of the Miocene, when uplift formed the Oman Mountains. Following Glennie *et al.* (1973, 1974), Coleman (1981) stated that the opposing rotation of Eurasia and Africa initiated the closing of the Tethyan Sea. This in turn caused the obduction of the ophiolite along a big NE dipping detachment fault in the Tethys Sea during Cenomanian time (93.5 – 99.6 Ma). The continuing closing of Tethys Sea exposed oceanic crust to extensive erosion above sea level, depressed the continental margin along Oman, and thrust oceanic and continental material underneath the Oman ophiolite [Coleman, 1981].

Boudier *et al.* (1988) also thought that the thrust fault that brought the ophiolite onto continental crust initiated at the spreading ridge (Figure 4) and listed the following three observations in support of this view. 1) The geometry of the ophiolite nappes indicates that the thrust fault is formed at a spreading ridge because the ophiolite series thickens to the northeast systematically. For example, at the Wadi Tayin cross-section, the thickness increases from 1 km at the southwestern part to 10-12 km at the northeastern part. Additionally, no major, low inclination tectonic discontinuity within the nappes is observed in field mapping, suggesting that the thickening is not caused by internal thrusting. Thus, the northeastward thickening of the ophiolite reflects the original thickness of the paleo-ridge. 2) The lithosphere was still hot when the detachment happened, indicating that the detachment happened at a spreading ridge. The N-S to NE-SW trending shear zones discovered in the peridotites and gabbros are related to the detachment and early thrusting. The plastic deformation of peridotites indicates the peridotites were hot enough to deform plastically during the detachment, probably above 800°C [Nicolas, 1986]. The magmatic activity in the shear zones also suggests hot lithosphere. For instance, in the Sumeini window, the partial melting of amphibolites produced a tonalitic melt [Searle and Maplas, 1980, 1982]. 3) The plagiogranites that intruded the ophiolites and the metamorphic sole overlap in age, which indicates the detachment started when the ridge was still active or right after the ophiolites were formed in the ridge.

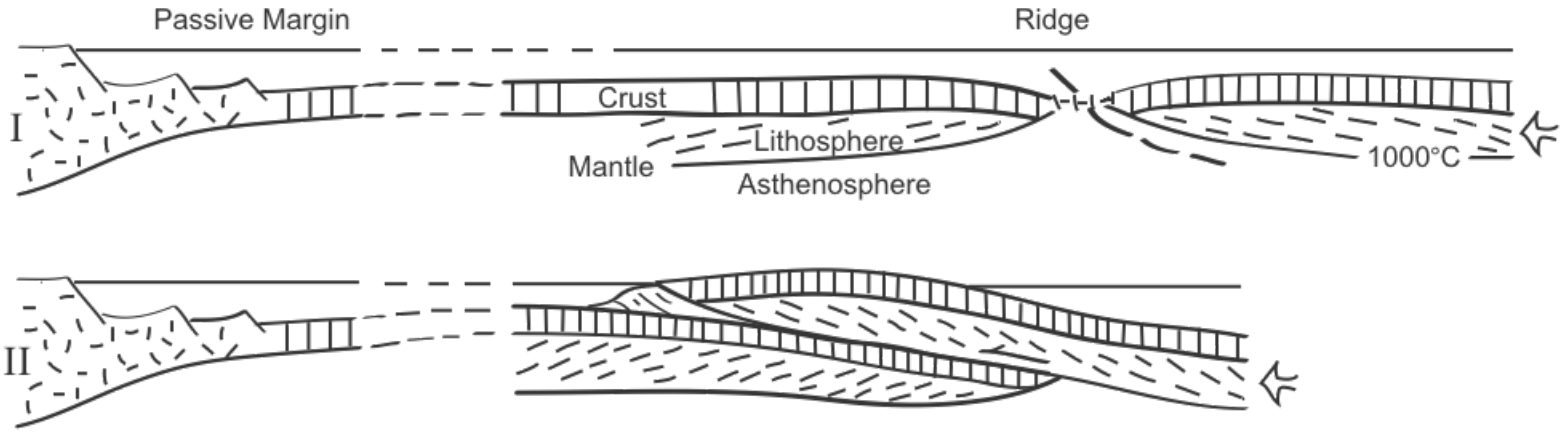

Figure 4. Schematic diagrams depicting detachment and initial emplacement of the Semail ophiolite. After Boudier (1988).

Nicolas (1989), listed three factors that favor a moderate to fast spreading ridge environment for the formation of the Oman ophiolite: 1) The layered gabbro sequence is thick and continuous, which suggests a permanent magma chamber that are found only beneath fast spreading ridge [Pallister and Hopson, 1981]. 2) With the exception of the transform fault in the Wadi-Tayin section, the absence of transform faults for over 300 km along the inferred ridge axis in Oman is comparable with East Pacific Rise (Figure 3.1 Nicolas 1989). 3) The foliations in the uppermost peridotites indicate the flow pattern was parallel to the Moho surface, which is a characteristic of a fast spreading ridge.

Benoit and others (1996) analyzed trace elements and Sr and Nd isotopes on 34 mafic cumulates from the mantle sequence of the Oman ophiolite including olivine gabbros, gabbronorites, gabbronorite dorites, troctolites, clinopyroxene troctolites and troctolitic gabbros. Although the trace element and isotope data varied between difference types of mafic cumulates, they found that this variation could be explained by various degree of fractional crystallization of MORB source liquid.

The interpretation that the Oman ophiolite formed at a mid-ocean ridge has been challenged by the discovery of secondary volcanism in central Oman. An alternative proposed tectonic setting for the formation of the Oman ophiolite is an island-arc environment or a back-arc basin [Pearce *et al*., 1981, 1984; Alabaster *et al*., 1982; Searle and Stevens, 1984; Lippard *et al.*, 1986]. Pearce *et al*. (1984) compared the trace element geochemistry of supra-subduction zone basalts and SSZ

ophiolites. If the ophiolites were formed in a SSZ environment, they should have geochemical features consistent with such basalts. Supra-subduction zone basalts are typically depleted in Ta and Nb. SSZ ophiolites also fall into island arc basalts region in the Th-Hf-Ta and Cr-Y discrimination diagram. Compared to MORB-type ophiolites, SSZ type ophiolites are depleted in Ta and Y. In addition to their distinct trace element geochemistry, Pearce *et al.* (1984) also concluded that SSZ ophiolites usually have a depleted harzburgite mantle sequence, and more abundant chromite podiform deposits. According to Pearce *et al.* (1984), the Oman ophiolite conforms to SSZ ophiolite characteristics for all of the above-mentioned criteria.

Pearce *et al.* (1984) argued that the Oman ophiolite formed at spreading ridge-arc transition environment because of the composition of its two main basalt lavas suites. The Lasail unit contains a large portion of rhyolites, dacites and andesites, which is not uncommon for a supra-subduction zone environment, whereas the Alley unit only contains a small portion of the felsic rocks, which is more typical of mid-ocean ridges [Pearce *et al.*, 1984].

Gray and others (2000) reported high-P low-T eclogite and blueschist facies metamorphic rocks in the Saih Hatat window. Eclogites and blueschists, which are absent in the rest of the Samail ophiolite, usually form in a subduction zone environment. In contrast with previous models that require a northeast dipping subduction zone, Gray and others (2000) have identified two shear zones within the Saih Hatat window that they interpret to be related to a southwest dipping subduction zone.

Searle and Cox (1999, 2002) also favor the SSZ model. The interpretation that a supra-subduction zone was the likely setting for the formation of the Samail ophiolite is based on the geochemistry of the metamorphic sole, the age of the formation of ophiolite and the metamorphic sole, and the peak P-T conditions of the metamorphic sole. The major and trace element geochemistry of metamorphic sole amphibolites from Asimah, Wadi-Tayin and Sumeini is similar to the geochemistry of the tholeiitic Haybi volcanic rocks, which are metamorphosed Triassic and Jurassic ocean floor basalts, but different from the upper volcanic unit of Samail ophiolite. The age of the ophiolite series and the age of the metamorphic soles are very similar, suggesting that the two tectonic units were formed contemporaneously. The Supra Subduction Zone model more realistically explains this age similarity (ages of the ophiolites and the metamorphic sole mentioned earlier in the introduction are from the following work: Hacker, 1994; Hacker *et al*., 1996; Tilton *et al*., 1981). Thermobarometric studies of metamorphic rocks from Wadi-Tayin, Sumeini and Asimah indicate that the peak P-T conditions were 870-840°C and 13.9-11.8 kbar. These pressures correspond to a depth of 54-46km beneath the surface of the Earth, a depth that cannot be explained by the thickness of the ophiolites and strongly suggests subduction.

The supra-subduction zone model can well explain the secondary magmatism and the eclogite facies rocks in Oman. Difficulties arise, however, in identify an associated trench and arc. Regardless of which kind of tectonic setting the Oman ophiolite formed in, there is no question that the ophiolites represent a slice of

oceanic lithosphere. As a result, the hydrothermal alteration information kept in Oman ophiolites is helpful in understanding the ongoing hydrothermal alteration in the oceanin lithosphere.

Gregory & Taylor (1981) published an ^{18}O profile of the Oman ophiolite, which has come to represent the classic and standard model of hydrothermal circulation, both in Oman and at mid-ocean ridges generally. They analyzed 75 samples from Ibra area and provided an ^{18}O profile in the crustal section. Their data showed that upper 75% of the crustal section has reacted with hydrothermal fluid. The fluid also locally penetrated into tectonized peridotites. A ship-shaped magma chamber was pictured in their paper. The deck of the ship is the boundary between sheeted dikes and massive gabbros. There was a circulation system above and below the boundary, respectively. The two hydrothermal circulation systems were decoupled at ridge system, which might be related to the difference in permeability: sheeted dikes are much more permeable than the massive gabbros. Their model was supported by the observed oxygen isotope profile. The pillow lavas and sheeted dikes are enriched in ^{18}O, while the gabbros are depleted in ^{18}O. The absence of hydrous alteration minerals in the gabbros, except for minor amount of talc or amphibole, indicates that the hydrothermal exchange happened at temperature >400~500°C. Similarly, hydrothermal fluid contamination of the lower gabbro section was proposed by Lanphere *et al.* (1981) and McCulloch *et al.* (1981) on the basis of Sr isotope analysis.

Since Greogry and Taylor's 1981 paper, considerable work has provided evidence of hydrothermal fluid circulation within the Oman ophiolite [Manning *et al.,* 2000; Kawahata *et al*., 2001; Nicolas *et al*., 2003; Bosch *et al*., 2004]. Manning *et al*. (2000) examined Hess Deep gabbroic rocks and the gabbros from Wadi Abyad section in the central part of the Oman ophiolite. Hess Deep (101°30'W, 2°15'N) is a submarine rift valley at the western end of the Cocos-Nazca spreading center. It is about 50-100 km east of present East Pacific Rise spreading axis [Hey *et al*., 1972; Manning *et al*., 1996]. Their calculated temperatures from amphibole and plagioclase ranged from 700°C in the dike-gabbro transition to 825°C in the lowest gabbro at the Moho. Kawahata *et al*. (2000) analyzed Sr isotope ratios on rocks from Wadi Fizh and concluded the temperature of hydrothermal alteration increased from basalt section (low temperature alteration) to cumulate gabbro section (amphibolite facies) from secondary mineral assemblage.

Nicolas *et al*. (2000) published a new structural map of the Oman ophiolite and confirmed that the greenschist hydrothermal veins are pervasive in the crustal section and aligned parallel to the sheeted dike complex [Bosch *et al*., 2004]. Bosch *et al*. (2004) performed extensive isotopic and petrological studies from 500 gabbro specimens from the entire ophiolites. All analyzed whole rocks and separated minerals have $^{87}Sr/^{86}Sr$ shifted to higher values than MORB (~0.7029). Oxygen isotope data showed that all samples have distinct ^{18}O values, compared with those from MORB (~5.7). A very interesting observation in their study is the extreme ^{18}O depletion in pyroxene and amphibole minerals separated from the samples. They

ascribed the extreme depletion as equilibrated exchange between these minerals and a hydrothermal fluid with very low $\delta^{18}O$. In addition to the isotopic study, they reported on the petrography of very high temperature (VHT), high temperature (HT) and low temperature (LT) mineral assemblages. The VHT alteration facies are represented by orthopyroxene coronas between olivine and plagioclase. The corresponding temperature is about 900~1000°C [Koepke *et al.,* 2003]. The HT alteration facies are represented by chlorite and pale amphibole coronas between olivine and plagioclase, as well as the iddingsite partially or totally replacing olivine. The alteration temperature is between 550°C and 900°C [Liou *et al*., 1974; Spear, 1981]. The LT alteration facies are represented by lizardite alteration of olivine, accompanied by saussurite in plagioclase. The alteration temperature is below 500°C. This is the only stage that plagioclase shows alteration [Bosch *et al*., 2004].

Alteration Mechanism

Nicolas *et al*. (2003) and Bosch *et al*. (2004) suggested these reactions and oxygen isotopic variations resulted from a hydrothermal circulation system below fast spreading ridge. Microcracks, gabbroic dikes, hydrothermal veins which have orientations parallel to that of sheeted dikes and normal to the mineral lineation are essentials in their hydrothermal alteration system. In their circulation model, which is based on the field observation of the foliation of gabbros, the magma chamber is a chimney shape with flaring bottom. The microcracks, which are about 0.1~0.2mm and filled with the same alteration minerals as those in the gabbro

section (as described by Bosch *et al*. 2004), are the recharge unit of HT/VHT hydrothermal system (Figure 5). The opening of the microcracks is controlled by the anisotropy of thermal expansion. The hydrated gabbroic dikes and plagiogranite dikes, which are the result of the hydrous remelting within the crust, are the discharge unit of HT/VHT hydrothermal system. The hydrated gabbro dikes grade into LT hydrothermal veins in the upper crust section. LT hydrothermal veins are not restricted to the upper crust section, rather they have been observed at all levels including the layered lower gabbro. The in situ cooling of the ophiolite for ~1 Ma can sweep down the 500°C isotherm down to the Moho level and develop LT alteration.

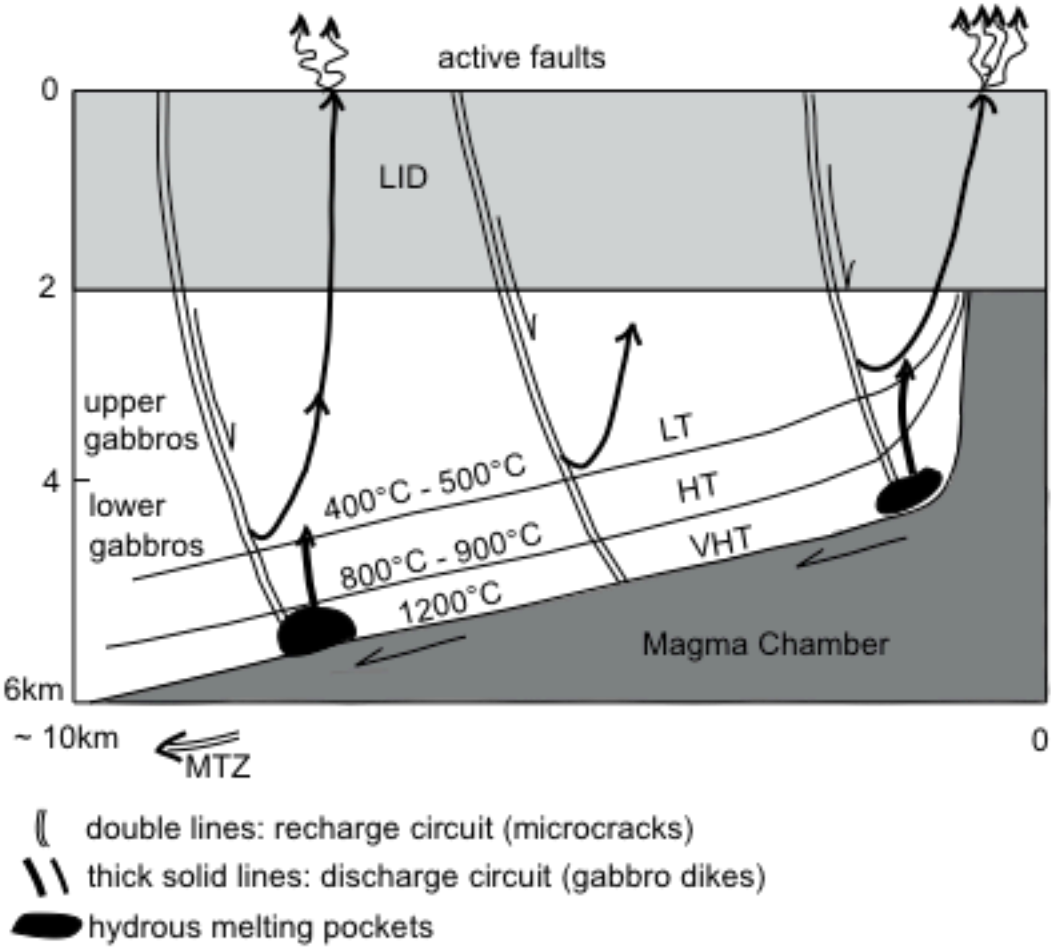

Figure 5. Model of hydrothermal circulation system at a fast spreading ridge. The microcracks are the recharge unit of hydrothermal system (double lines). The hydrated gabbroic dikes, which are the result of the hydrous remelting within the crust, are the discharge unit (thick solid lines). From Nicolas *et al.*, 2003.

METHODS

Sampling

The fieldwork was conducted in February 2010 by Professor Christopher Andronicos and Professor Lawrence Cathles in the Oman mountains. Thirty-three rocks were collected from the Wadi-Tayin, Nakhl and Sumail nappes, sampling a transect of ophiolite from upper gabbro to Moho Transition Zone. The localities and GPS positions of the samples are summarized in Table 1. This study was designed to understand hydrothermal alteration system within the oceanic lithosphere. In this study, the cracks and veins are thought to control the degree of alterations. To achieve this, a range of samples were collected, from the freshest rocks that are not affected by fractures or veins, to samples that are near fractures and veins, and to samples from cracks and veins

Fresh pieces were cut from each sample on a diamond saw, grinded into rock chips on a rock grinding machine, and powdered in a ceramic shatterbox for major element, trace element and isotopic analysis.

Major Elements

Major element analyses were performed by electron microprobe (JEOL-8900 superprobe, Cornell Center for Materials Research) on glasses made from rock powders. Techniques and standards for microprobe analyses of major elements are from Kay *et al.* (1987). Gabbros were melted in a molybdenum strip furnace in an Ar atmosphere. Microprobe analyses were done at 15 kV with a current of 15 nA using

Table 1. Locations of sampled Oman ophiolite (longitude and latitude), position of each sample in gabbroic sections, and corresponding rock types.

Sample Name	Nappe	Locations	Location in the gabbroic section	Distance to Moho	Type of Rock
OM45	Wadi-Tayin	22°52'19.8",58°38'30.8"	Upper Gabbro	4.2 km	gabbro
OM46	Wadi-Tayin	22°52'19.5",58°38'30.2"	Upper Gabbro	4.2 km	gabbro
OM47	Wadi-Tayin	22°52'20.0",58°38'30.8"	Upper Gabbro	4.2 km	gabbro
OM48	Wadi-Tayin	22°52'20.2",58°38'30.4"	Upper Gabbro	4.2 km	peridotite
OM40	Wadi-Tayin	23°52'42",58°36'46.7"	Middle Gabbro	3 km	peridotite
OM40A	Wadi-Tayin	23°52'42",58°36'46.7"	Middle Gabbro	3 km	gabbro
OM40B	Wadi-Tayin	23°52'42",58°36'46.7"	Middle Gabbro	3 km	gabbro
OM15A	Wadi-Tayin	22°53'18.7",58°31'27.0"	Middle Gabbro	1.8 km	gabbro
OM15B	Wadi-Tayin	22°53'18.7",58°31'27.0"	Middle Gabbro	1.8 km	gabbro
OM16	Wadi-Tayin	22°53'21.77",58°31'35.1"	Middle Gabbro	1.8 km	gabbro
OM19	Wadi-Tayin	22°53'37.5",58°32'6.7"	Middle Gabbro	1.8 km	gabbro
OM9A	Sumail	23°5'58.7",58°5'19.0"	Lower Gabbro	0.6 km	gabbro
OM9B	Sumail	23°5'58.7",58°5'19.0"	Lower Gabbro	0.6 km	gabbro
OM31	Sumail	23°5'58.1",58°5'18.9"	Lower Gabbro	0.6 km	gabbro
OM33	Sumail	23°5'58.2",58°5'16.9"	Lower Gabbro	0.6 km	gabbro
OM34	Sumail	23°5'59.3",58°5'19.9"	Lower Gabbro	0.6 km	gabbro
OM35	Sumail	23°5'58.8",58°5'19.9"	Lower Gabbro	0.6 km	gabbro
OM37A	Sumail	23°5'53.1",58°5'14.3"	Lower Gabbro	0.6 km	gabbro
OM37B	Sumail	23°5'53.1",58°5'14.3"	Lower Gabbro	0.6 km	quartz vein in gabbro
OM38	Sumail	23°5'58.6",58°5'8.6"	Lower Gabbro	0.6 km	gabbro
OM39	Sumail	23°5'57.5",58°5'13.5"	Lower Gabbro	0.6 km	gabbro
OM28	Sumail	23°5'35.5",58°6'13.6"	Lower Gabbro	0.6 km	gabbro
OM49	Nakhl	23°26'36.6",57°39'24.9"	Moho		peridotite
OM49A	Nakhl	23°26'36.4",57°39'25.2"	Moho		peridotite
OM49B	Nakhl	23°26'36.4",57°39'25.2"	Moho		peridotite
OM50	Nakhl	23°26'36.5",57°39'31.4"	Moho		gabbro
OM7	Sumail	23°2'52.8", 57°54'0.6"	MTZ		dunite
OM8	Sumail	23°2'58.2", 57°54'2.2"	MTZ		magnesite
OM8A	Sumail	23°2'58.2", 57°54'2.2"	MTZ		dunite
OM8C	Sumail	23°2'58.2", 57°54'2.2"	MTZ		magnesite
OM8E	Sumail	23°2'52", 57°53'57.6"	MTZ		gabbro
OM8F-1	Sumail	23°2'52", 57°53'57.6"	MTZ		peridotite
OM8F-2	Sumail	23°2'52", 57°53'57.6"	MTZ		gabbro
OM8G	Sumail	23°2'52", 57°53'57.6"	MTZ		gabbro
OM8H	Sumail	23°2'52", 57°53'57.6"	MTZ		gabbro

wavelength dispersive spectrometers. Standards a99 (olivine crystal), Juan de Fuca glass and Kakanui hornblende were treated as unknowns. Analysis results are reported in Table 2.

Trace Elements

Trace element concentrations were measured at Cornell University using an inductively coupled plasma mass spectrometer (ICP-MS) with a Varian SPS3 Auto-sampler. Techniques and standards have been described by Kay et al. (1987), Cheatham et al. (1993), and White & Duncan (1996). Approximately 50 mg of sample powder and external calibration standard powders (BEN, BHVO-2, BCR-2, BIR-1) were dissolved via hot plate digestion for 24 hours using a mixture of 4B HF and concentrated perchloric acid ($HClO_4$) in closed Savillex® containers. Digestions were dried down after dissolution and re-dissolved twice in 6 N QD HCl to remove remaining fluorides. Samples were converted to nitrate-form by re-dissolution in 2 ml of QD HNO_3 and dried down. Samples were re-dissolved in 1 ml of 2% HNO_3 and diluted to 200 g (approximately 0.025% total dissolved solids). Twenty-two trace elements (Cs, Ba, La, Ce, Pr, Nd, Sm, Eu, Gd, Tb, Dy, Ho, Er, Tm, Yb, Lu, Hf, Ni, Sr, Zr, Rb, Y) were analyzed on each sample. Analytical runs consisted of blank measurements in the beginning and at the end, four standards (BEN, BIR-1, BCR-2 and BHVO-2) in the beginning and at the end, two of the standards (BEN and BIR-1) in the middle and ten samples with unknown trace element concentrations. External standards BEN and BIR-1 were run in the beginning and every five

Table 2. Major element data for standards a99, Juan de Fuca glass and Kaknui hornblende.

	a99					
	Run 1	Run 2	Run 3	Run 4	Average	Recommended
SiO_2	51.07	51.18	51.27	51.03	51.14	50.94
TiO_2	4.07	4.06	4.06	4.02	4.05	4.06
Al_2O_3	12.37	12.47	12.47	12.58	12.47	12.49
FeO	12.95	13.86	13.71	13.90	13.61	13.32
MnO	0.19	0.20	0.19	0.19	0.19	0.19
MgO	5.04	5.06	5.09	5.05	5.06	5.08
CaO	8.99	8.95	8.75	8.91	8.90	9.30
Na_2O	3.04	2.97	3.00	2.86	2.97	2.66
K_2O	0.83	0.85	0.83	0.84	0.84	0.82
P_2O_5	0.55	0.51	0.44	0.43	0.48	0.38
Cr_2O_3	0.01	0.01	0.00	0.00	0.01	
Total	99.12	100.13	99.83	99.79	99.72	

	Juan de Fuca glass					
	Run 1	Run 2	Run 3	Run 4	Average	Recommended
SiO_2	50.53	50.51	50.76	50.54	50.59	50.81
TiO_2	1.85	1.82	1.86	1.85	1.84	1.85
Al_2O_3	13.77	14.03	13.96	13.99	13.93	14.06
FeO	11.30	12.20	12.14	12.22	11.96	11.88
MnO	0.21	0.23	0.20	0.20	0.21	0.22
MgO	6.95	6.99	7.00	6.98	6.98	6.71
CaO	10.88	10.84	10.55	10.63	10.73	11.12
Na_2O	2.76	2.80	2.80	2.78	2.79	2.62
K_2O	0.18	0.19	0.19	0.18	0.19	0.19
P_2O_5	0.28	0.27	0.22	0.19	0.24	0.20
Cr_2O_3	0.01	0.00	0.03	0.02	0.01	
Total	98.72	99.89	99.70	99.58	99.48	

	Kaknui Hornblende					
	Run 1	Run 2	Run 3	Run 4	Average	Recommended
SiO_2	40.74	40.75	40.72	40.80	40.75	40.37
TiO_2	4.82	4.82	4.84	4.84	4.83	4.72
Al_2O_3	14.23	14.43	14.40	14.36	14.35	14.90
FeO	10.53	11.28	11.14	11.09	11.01	10.92
MnO	0.07	0.11	0.10	0.08	0.09	0.09
MgO	12.63	12.72	12.71	12.68	12.68	12.80
CaO	10.08	9.92	9.73	9.77	9.87	10.30
Na_2O	2.71	2.72	2.68	2.69	2.70	2.60
K_2O	2.02	2.12	2.08	2.08	2.08	2.05
P_2O_5	0.06	0.05	0.06	0.05	0.06	
Cr_2O_3	0.00	0.01	0.00	0.00	0.00	
Total	97.89	98.92	98.46	98.45	98.43	

samples to monitor the analytical precision. Standard BEN was used to conduct drift correction on all the data. The drift correction method has been described by Cheatham *et al*. (1993). The other three standards are treated as unknown samples, and their concentrations were calculated and compared to recommended values to evaluate the accuracy of the analysis (Table 3).

Isotope Ratios

Sample preparation and analytical methodology for Sr isotopic analysis was similar to White and Duncan (1996). Samples (~50 mg for each sample) were dissolved via hot plate digestion for 24 hours in a mixture of Teflon-distilled HF and concentrated perchloric acid ($HClO_4$) in closed Savillex® containers. Digestions were dried and re-dissolved twice in 6 N QD HCl. Samples were then dissolved in 2.5 N QD HCl and centrifuged for 5 minutes at 5000 rpm prior to column chemistry. Sr was separated by elution with 2.5 N HCl from AG50W-x8 (200-400 mesh) resin cation exchange columns. Sr isotopic ratios were measured at the Keck Isotope Laboratory at Cornell University using a VG Sector 54 thermal ionization mass spectrometer (TIMS) operating in dynamic mode. Isotopic ratios were normalized to $^{88}Sr/^{86}Sr=0.11940$, using an exponential correction. During the period of analysis the NBS-987 Sr standard yielded $^{87}Sr/^{86}Sr = 0.71023 \pm 0.00002$ (2σ) (n=7).

Leaching experiments were performed on samples with $^{87}Sr/^{86}Sr > 0.7074$. Samples were crushed into rock chips and the pieces with diameters of 1-2 mm were handpicked. Approximately 50 mg of each sample was immersed in pure glacial

Table 3. Trace element data of standards BEN, BIR-1, BCR-2 and BHVO-2. BEN was used to conduct drift correction. Concentrations of standards in this analysis are comparable to published values. Mass number after each element represents the isotope being analyzed. Concentrations are reported in ppm for each element.

	BEN			**BIR-1**			**BCR-2**		**BHVO-2**	
	mid-run	end-run	Recommend	mid-run	end-run	Recommend	end-run	Recommend	end-run	Recommend
Cs (133)	0.72	0.72	0.8	0.02	0.02	0.005	1.20	1.1	0.12	0.10
Rb (85)	45.13	45.13	47	0.64	0.66	0.186	51.02	46.9	9.52	9.80
Ba (138)	1013.82	1013.82	1025	5.92	4.50	6.63	733.71	677	126.66	129.00
La (139)	81.52	81.52	82	-0.21	-0.34	0.556	27.54	24.9	15.68	15.10
Ce (140)	152.03	152.03	152	2.44	2.04	1.897	55.51	52.9	36.23	36.60
Pr (141)	17.38	17.38	17.5	0.27	0.19	0.39	7.22	6.57	5.38	5.40
Sr (88)	1367.67	1367.67	1370	99.56	98.34	110.8	345.34	340	381.82	389.00
Nd (146)	66.85	66.85	67	2.37	1.94	2.402	30.82	28.7	25.24	25.40
Zr (91)	273.48	273.48	260	31.64	31.46	22	172.84	188	170.70	172.00
Hf (177)	6.16	6.16	5.6	0.85	0.73	0.58	4.46	4.8	4.44	4.67
Sm (147)	12.15	12.15	12.2	1.07	0.86	1.106	7.06	6.57	6.24	6.17
Eu (151)	3.61	3.61	3.6	0.54	0.46	0.522	2.08	1.96	1.95	2.06
Gd (157)	10.11	10.11	9.7	2.40	2.20	1.98	6.56	6.75	5.74	6.13
Tb (159)	1.31	1.31	1.3	0.41	0.35	0.41	1.04	1.07	0.91	0.88
Dy (163)	6.40	6.40	6.4	2.67	2.18	2.62	6.61	6.41	5.46	5.38
Ho (165)	1.09	1.09	1.1	0.59	0.49	0.587	1.34	1.3	1.02	1.00
Y (89)	28.41	28.41	30	16.34	16.20	16	38.24	37	26.83	26.00
Er (167)	2.54	2.54	2.5	1.72	1.40	1.71	3.75	3.66	2.55	2.54
Tm (169)	0.33	0.33	0.34	0.26	0.21	0.27	0.58	0.564	0.36	0.33
Yb (174)	1.94	1.94	1.8	1.62	1.36	1.7	3.51	3.38	2.13	2.06
Lu (175)	0.26	0.26	0.24	0.24	0.20	0.26	0.54	0.519	0.29	0.28
Ni (58)	259.73	259.73	267	171.08	173.76	166	7.86	10.8	123.19	119

Unit: ppm

acetic acid in a closed Savillex® container on a hot plate for two hours. The reason of dissolving samples in acetic acid is that the weak acid can dissolve carbonates without dissolving the rock. The leachate was removed with a pipette and transferred to separate Savillex® containers. Sample residues were rinsed several times; the rinsing solution was collected and transferred to the Savillex® containers containing the leachate. Rock residues and carbonate solutions were then dried on a hot plate. The rock residues were dissolved using the above procedure. $^{87}Sr/^{86}Sr$ ratios of the carbonates and the rock residues were then measured.

$\delta^{18}O$ values were analyzed on VG Micromass gas source stable isotope ratio mass spectrometers at Geochron Laboratories in Massachusetts. Replicate samples were analyzed to evaluate accuracy and precision.

RESULTS

Major Elements

Major element analyses of 28 samples are reported in Table 4. CIPW norms, calculated using the "Norm4" spreadsheet written and distributed by Kurt Hollocher of Union College are listed in Table 5. Using a total alkali-silica classification system [Cox et al., 1979], all samples are subalkaline/tholeiitic with most samples classified as gabbro while samples from MTZ and Moho fall into the field of ultrabasic rocks. Figure 6 is the Google map locations of sampled lower gabbros from Wadi Samarh in Sumail Nappe: OM9A, OM9B, OM31, OM33, OM34, OM35, OM37A, OM38, OM39. Figure 7 shows major oxides plotted against MgO for these lower gabbros. Among the samples, OM9A, OM9B, OM31, OM33, OM34 and OM35 are from a 150 m long outcrop. Except OM 33, all the rest gabbros from this outcrop are within 10 m of vertical distance and 50 m of horizontal distance. One robust assumption is that these rocks from the same gabbro layer have the same starting composition. Samples OM37A, OM38 and OM39 are from nearby outcrops in the same wadi, within the distance of 250 m. It is not safe to make the same assumption that they start with the same compositions as the other ones. However, because those samples are very close to the big outcrop (within a few hundred meters), the starting composition and mineral assemblage should be similar. Thus, differences in chemical composition should be due to the hydrothermal alteration. The amount of SiO_2, FeO, MnO, Cr_2O_3 (wt %) and Ni (ppm) increase with the

Table 4. Major element data from electron microprobe analysis for the Oman ophiolite. Total Fe reported as Fe^{2+}.

	Upper Gabbro			**Middle Gabbro**						**Lower Gabbro**				
	OM46	OM47	OM48	OM40	OM40A	OM40B	OM15A	OM15B	OM16	OM19	OM9A	OM9B	OM31	OM33
SiO_2	48.62	47.12	47.30	47.58	47.90	48.18	43.01	45.81	47.84	44.01	47.64	48.52	46.40	48.25
TiO_2	0.28	0.10	0.27	0.23	0.26	0.23	0.06	0.08	0.24	0.05	0.24	0.35	0.23	0.25
Al_2O_3	21.29	32.11	17.40	19.51	15.52	20.01	17.97	20.70	15.49	23.42	17.03	14.58	20.92	16.65
FeO	3.41	1.02	4.43	3.54	5.41	3.78	7.09	6.53	6.13	1.06	5.90	5.78	4.02	5.13
MnO	0.07	0.01	0.08	0.07	0.10	0.06	0.10	0.09	0.11	0.04	0.11	0.10	0.08	0.08
MgO	7.55	0.84	11.72	9.91	12.81	9.01	15.64	13.92	12.38	2.67	11.12	11.18	8.33	10.84
CaO	16.95	15.85	16.77	17.63	16.59	16.81	12.99	11.72	15.42	25.56	16.29	17.40	17.04	16.95
Na_2O	1.59	2.19	1.06	1.01	0.86	1.24	0.29	1.27	0.99	0.03	0.98	0.82	0.84	0.84
K_2O	0.02	0.02	0.05	0.03	0.01	0.03	0.01	0.01	0.03	0.00	0.00	0.01	0.11	0.03
P_2O_5	0.02	0.05	0.06	0.06	0.05	0.06	0.05	0.04	0.05	0.10	0.05	0.05	0.04	0.05
Cr_2O_3	0.05	0.00	0.04	0.05	0.13	0.04	0.02	0.06	0.04	0.06	0.04	0.11	0.02	0.04
Total	99.84	99.31	99.17	99.63	99.65	99.45	97.23	100.25	98.73	96.99	99.40	98.90	98.04	99.11

	Lower Gabbro *continued*						**Moho**		**MTZ**				
	OM34	OM35	OM37A	OM37B	OM38	OM39	OM28	OM49A	OM50	OM8E	OM8F-2	OM8G	OM8H
SiO_2	46.53	47.52	46.99	45.93	42.51	42.57	47.71	48.98	47.33	47.22	42.40	37.67	49.50
TiO_2	0.21	0.25	0.17	0.15	0.57	0.17	0.81	1.41	0.13	0.11	0.09	0.07	0.05
Al_2O_3	16.80	16.49	20.01	20.19	14.58	18.53	17.85	16.21	12.44	17.07	19.17	28.53	15.71
FeO	6.63	6.44	4.24	2.77	7.40	3.25	5.82	9.96	3.28	4.65	5.26	7.49	3.82
MnO	0.11	0.12	0.08	0.09	0.09	0.05	0.09	0.18	0.10	0.09	0.11	0.05	0.08
MgO	11.67	11.67	9.94	4.50	9.55	7.45	9.98	8.47	10.02	13.85	14.13	4.19	12.90
CaO	15.50	16.79	16.70	25.83	13.96	14.04	14.45	12.07	25.14	16.62	15.78	20.08	15.42
Na_2O	0.91	0.81	1.03	0.07	1.08	1.48	1.45	2.65	0.13	0.66	0.09	0.03	1.45
K2O	0.01	0.01	0.01	0.00	0.01	0.02	0.03	0.11	0.00	0.01	0.01	0.00	0.01
P_2O_5	0.04	0.04	0.04	0.06	0.03	0.05	0.07	0.13	0.08	0.05	0.04	0.07	0.05
Cr_2O_3	0.06	0.04	0.00	0.01	0.04	0.01	0.06	0.02	0.09	0.11	0.17	0.03	0.09
Total	98.46	100.18	99.22	99.61	89.83	87.63	98.32	100.19	98.74	100.43	97.25	98.23	99.06

Unit: wt%

Table 5. Calculated CIPW norms of sampled Oman ophiolite. Calculation is conducted using the "Norm4" spreadsheet written and distributed by Kurt Hollocher of Union College.

	Upper Gabbro		Middle Gabbro							
	OM46		OM47		OM48		OM40		OM40A	
Normative Minerals	Weight %	Volume %	Weight %	Volume %	Weight %	Volume %	Weight %	Volume %	Weight %	Volume %
Plagioclase	64.11	68.57	96.04	96.84	50.37	55.11	56.4	60.97	45.94	50.94
Orthoclase	0.12	0.13	0.12	0.13	0.3	0.35	0.18	0.21	0.06	0.07
Nepheline	0.17	0.2	0.45	0.49	0.86	1.01	0.53	0.61		
Leucite										
Diopside	26.42	23.54	0.49	0.4	32.27	29.57	30.65	27.78	34.86	32.3
Hypersthene									2.51	2.29
Wollastonite										
Olivine	8.04	6.87	2.43	1.85	14.82	13.09	11.09	9.71	15.14	13.47
Larnite										
Ilmenite	0.53	0.33	0.19	0.11	0.51	0.32	0.44	0.27	0.49	0.32
Magnetite	0.55	0.31	0.16	0.08	0.72	0.42	0.57	0.32	0.87	0.51
Apatite	0.05	0.04	0.12	0.1	0.14	0.13	0.14	0.13	0.12	0.11

	Middle Gabbro *continued*									
	OM40B		OM15A		OM15B		OM16		OM19	
Normative Minerals	Weight %	Volume %	Weight %	Volume %	Weight %	Volume %	Weight %	Volume %	Weight %	Volume %
Plagioclase	59.78	64.43	51.56	56.84	61.36	66.6	46.71	51.87	65.79	68.64
Orthoclase	0.18	0.2	0.06	0.07	0.06	0.07	0.18	0.21		
Nepheline									0.14	0.15
Leucite										
Diopside	27.28	24.55	13.52	12.51	5.69	5.14	31.15	28.79	17.96	15.8
Hypersthene	2.37	2.1	4.14	3.75	5.02	4.45	6.54	5.92		
Wollastonite									10.34	10.41
Olivine	9.21	7.97	29.33	25.96	26.58	22.96	13.86	12.23		
Larnite									5.27	4.64
Ilmenite	0.44	0.27	0.11	0.07	0.15	0.09	0.46	0.29	0.09	0.06
Magnetite	0.61	0.35	1.17	0.69	1.04	0.6	1	0.58	0.17	0.1
Apatite	0.14	0.13	0.12	0.11	0.09	0.09	0.12	0.11	0.23	0.21

Table 5 *(continued)*

	Lower Gabbro									
	OM9A		OM9B		OM31		OM33		OM34	
Normative Minerals	Weight %	Volume %	Weight %	Volume %	Weight %	Volume %	Weight %	Volume %	Weight %	Volume %
Plagioclase	50.63	55.81	43.51	48.51	61.29	65.84	49.1	54.06	50.18	55.48
Orthoclase	0	0	0.06	0.07	0.65	0.75	0.18	0.21	0.06	0.07
Nepheline	0	0	0	0	0	0	0	0	0	0
Leucite										
Diopside	30.95	28.39	40.4	37.52	25.48	22.88	34.02	31.27	28.43	26.14
Hypersthene	3.6	3.23	5.94	5.4	1.76	1.55	6.29	5.67	3.13	2.81
Wollastonite										
Olivine	13.29	11.61	8.36	7.41	9.61	8.25	8.97	7.89	16.63	14.52
Larnite										
Ilmenite	0.46	0.29	0.66	0.43	0.46	0.28	0.49	0.31	0.4	0.25
Magnetite	0.96	0.56	0.94	0.55	0.67	0.38	0.83	0.48	1.09	0.63
Apatite	0.12	0.11	0.12	0.11	0.09	0.09	0.12	0.11	0.09	0.09

	Lower Gabbro *continued*									
	OM35		OM37A		OM38		OM39		OM28	
Normative Minerals	Weight %	Volume %	Weight %	Volume %	Weight %	Volume %	Weight %	Volume %	Weight %	Volume %
Plagioclase	48.06	53.27	58.92	63.67	49.01	54.69	64.34	68.89	55.34	60.66
Orthoclase	0.06	0.07	0.06	0.07	0.12	0.14	0.12	0.13	0.18	0.21
Nepheline	0	0	0.1	0.12	0	0	0	0	0	0
Leucite										
Diopside	33.3	30.73	26.21	23.67	30.74	28.31	23.16	20.64	23.7	21.55
Hypersthene	1.82	1.64	0	0	1.67	1.49	0.15	0.13	8.24	7.33
Wollastonite										
Olivine	15.15	13.3	13.61	11.79	15.86	13.72	11.12	9.51	9.88	8.57
Larnite										
Ilmenite	0.47	0.3	0.32	0.2	1.2	0.77	0.38	0.23	1.56	0.98
Magnetite	1.03	0.6	0.7	0.4	1.33	0.78	0.59	0.33	0.96	0.55
Apatite	0.09	0.09	0.09	0.09	0.09	0.09	0.14	0.13	0.16	0.15

Table 5 *(continued)*

	Moho		MTZ									
	OM49A		OM50		8E		8F-2		OM8G		OM8H	
Normative Minerals	Weight %	Volume %	Weight %	Volume %	Weight %	Volume %	Weight %	Volume %	Weight %	Volume %	Weight %	Volume %
Plagioclase	54.26	60.69	33.8	37.75	49.01	53.84	53.4	58.24	79.08	80.69	49.09	53.94
Orthoclase	0.65	0.77			0.06	0.07					0.06	0.07
Nepheline			0.6	0.72			0.41	0.49	0.14	0.15		
Leucite							0.05	0.06				
Diopside	21.99	19.94	53	50.03	30.49	28.13	17.28	15.9			31.91	29.27
Hypersthene	4.32	3.78			0.16	0.14					4.96	4.5
Wollastonite												
Olivine	14.23	11.92	3.81	3.48	19.24	17.15	26.1	23.12	16.62	12.45	13.15	11.69
Larnite			7.82	7.37			1.62	1.49	6.73	5.8	0.09	0.06
Ilmenite	2.66	1.69	0.25	0.16	0.21	0.13	0.17	0.11	0.13	0.08	0.62	0.36
Magnetite	1.59	0.93	0.54	0.32	0.74	0.43	0.87	0.5	1.23	0.67	0.12	0.11
Apatite	0.3	0.28	0.19	0.18	0.12	0.11	0.09	0.09	0.19	0.16		

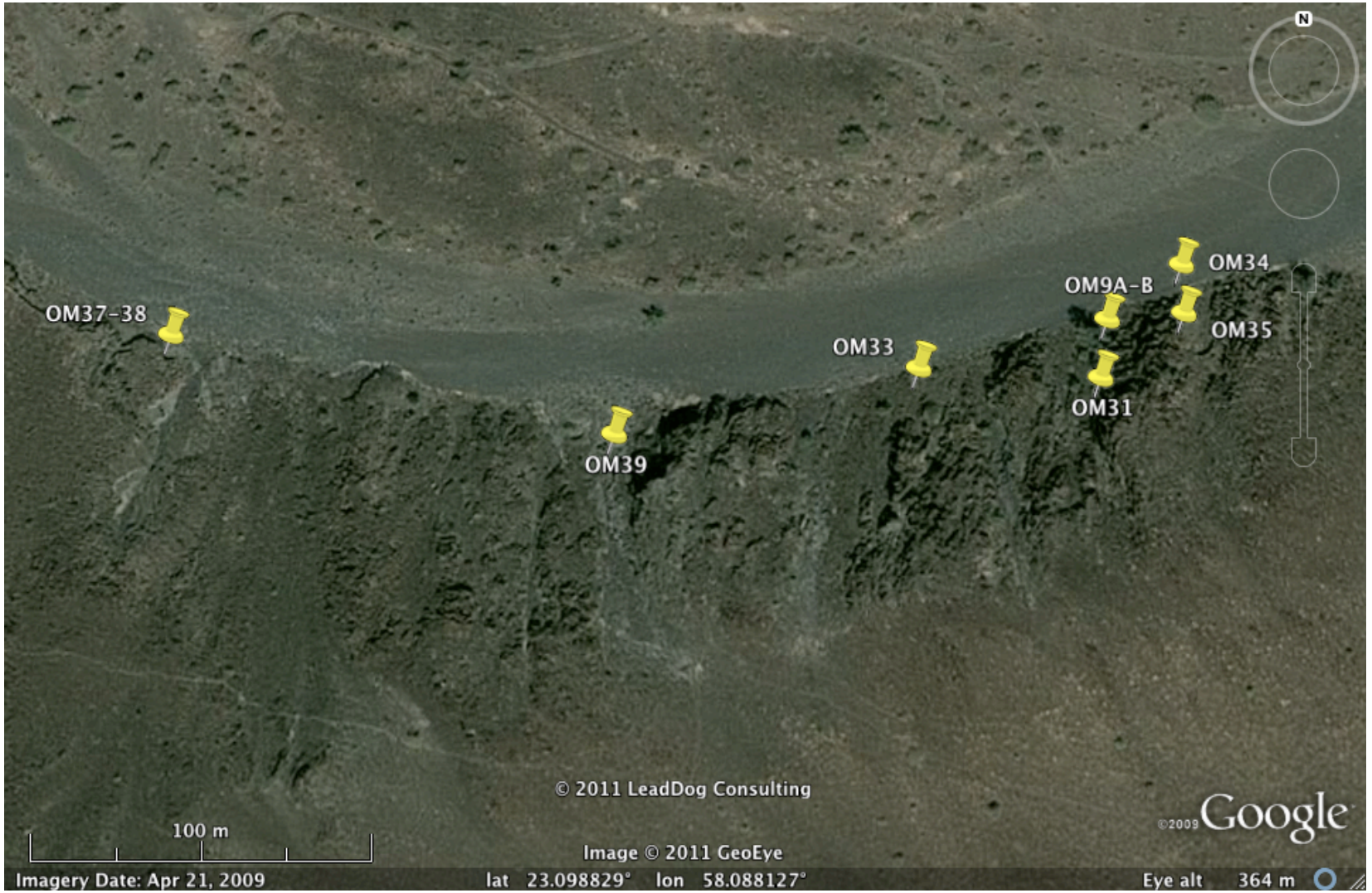

Figure 6. Relative locations of sampled lower gabbros from Wadi Samarh in Sumail nappe. OM9A, OM9B, OM31, OM33, OM34 and OM35 were sampled from the same layer of rocks. OM37A, OM38 and OM39 are from nearby outcrops.

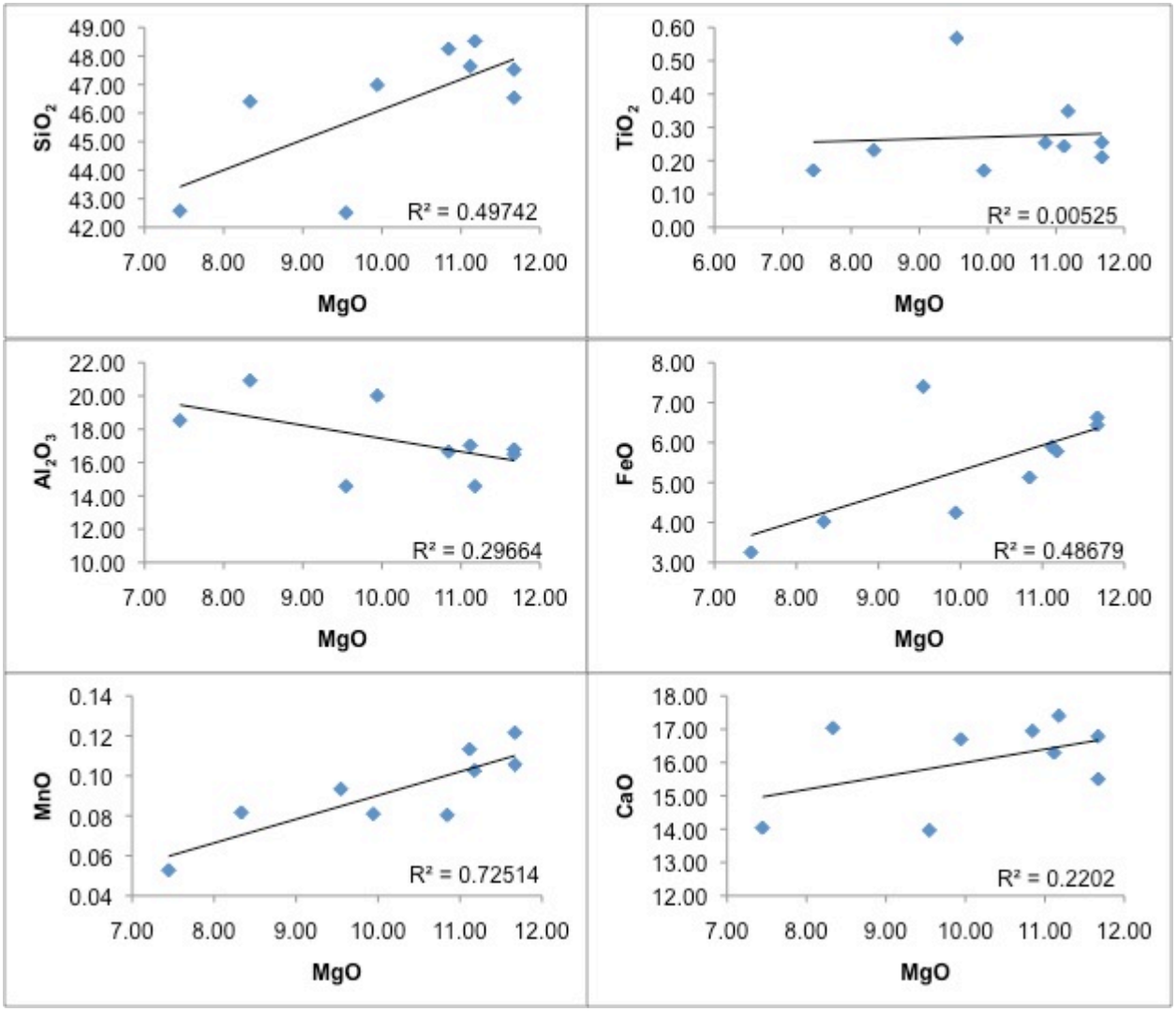

Figure 7. Bivariate diagrams of major elements/MgO. Samples are from lower gabbro section in Sumail nappe. The concentrations of SiO_2, FeO, MnO, Cr_2O_3 and Ni increase as the amount of MgO increases. Al_2O_3 and Na_2O decrease as the amount of MgO increases. TiO_2, K_2O and P_2O_5 don't show obvious trend.

Figure 7 *(continued)*

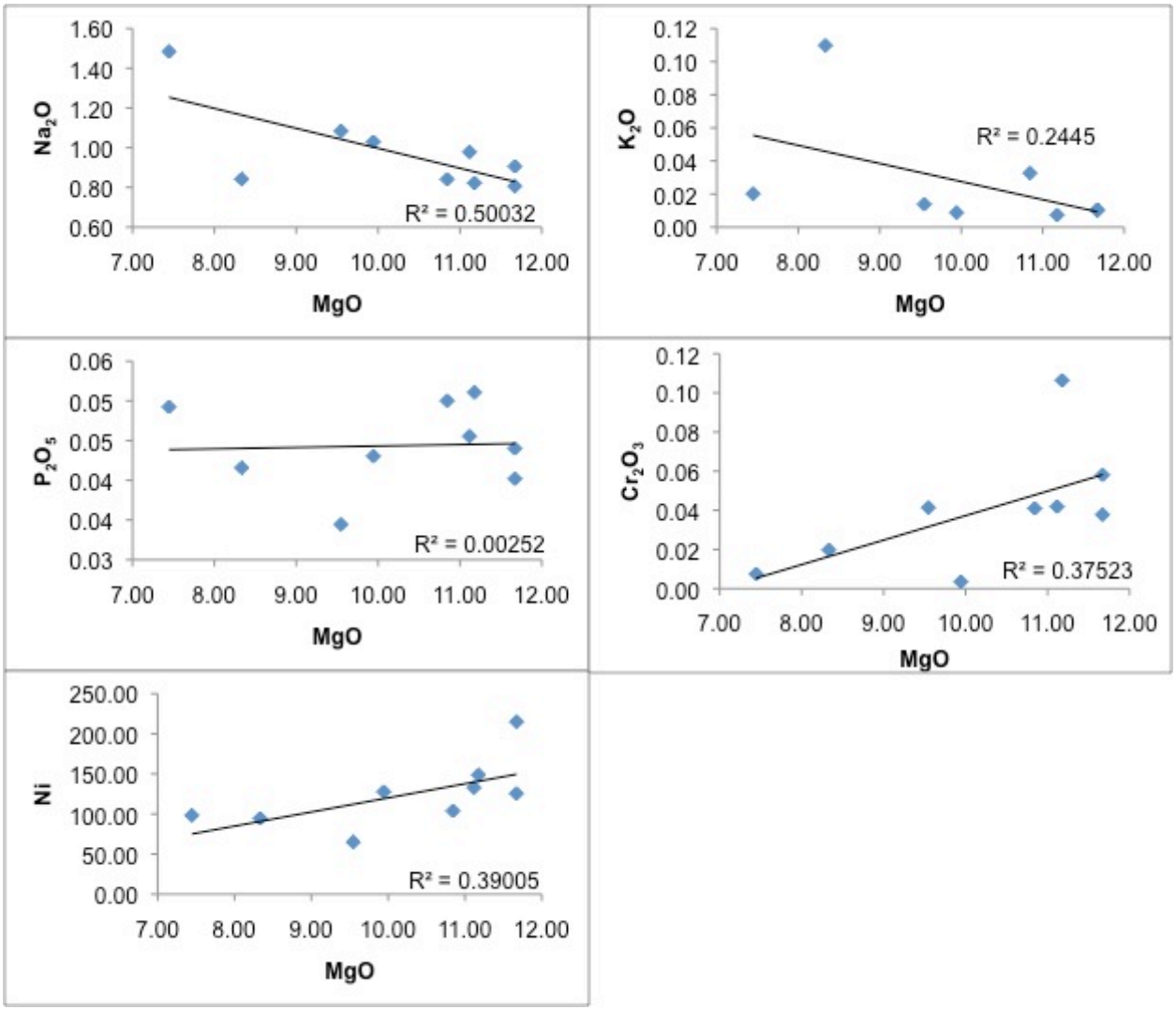

increase of MgO, while Al_2O_3 and Na_2O concentration decrease as the increase of MgO. TiO_2, CaO or P_2O_5 don't show systematic change with the change of MgO.

Trace Elements

Trace element analyses were performed on the samples from the cross section located at Wadi Samarh in Sumail Nappe and results are reported in Table 6. Concentrations of La in samples are too low during analysis, and were not reported here. With the exception of Sr, which is at same level as the concentration in MORB, incompatible elements are depleted in all samples relative to average MORB (Figure 8). As expected given their proximity in the field, the overall pattern is similar for all samples. In the MORB normalized REE plot, the samples are depleted in all REE elements, compared to MORB (Figure 9).

Isotope Analysis

Thirty-two samples were analyzed for $^{87}Sr/^{86}Sr$ and thirty-five samples for $\delta^{18}O$; results are listed in Table 7. Values range as follows: (1) upper gabbros, $^{87}Sr/^{86}Sr$ 0.7032~0.7080, $\delta^{18}O$ 2.4~6.3; (2) middle gabbros, $^{87}Sr/^{86}Sr$ 0.7031~0.7060, $\delta^{18}O$ 5.3~6.1; (3) lower gabbros, $^{87}Sr/^{86}Sr$ 0.7031~0.7064, $\delta^{18}O$ 3.4~6.7; (4) Moho peridotites and carbonates, $^{87}Sr/^{86}Sr$ 0.7035 ~ 0.7086, $\delta^{18}O$ 2.95 ~ 30.57. Figure 10 shows the change of Sr isotopic ratios with the change of depth, and Figure 11 shows the change of $\delta^{18}O$ with the change of depth. Among all the analyzed samples, six samples have $^{87}Sr/^{86}Sr > 0.7074$, which is the Cretaceous seawater value at 95Ma [McArthur *et al.*, 2001]. Five out of six with $^{87}Sr/^{86}Sr > 0.7074$ are

Table 6. Trace element data of the Oman samples from the secsion of lower gabbro. Mass number after each element represents the isotope being analyzed. Concentrations are reported in ppm for each element.

	Lower Gabbro								
	OM9A	OM9B	OM31	OM33	OM34	OM35	OM37A	OM38	OM39
Cs (133)	0.01	0.01	0.02	0.02	0.01	0.01	0.01	0.02	0.01
Rb (85)	0.38	0.47	0.68	0.50	0.39	0.39	0.38	0.42	0.39
Ba (138)	8.08	9.17	12.60	6.56	6.09	7.19	5.28	16.76	8.78
Ce (140)	1.99	2.29	1.91	2.00	1.79	1.95	1.78	2.05	1.82
Pr (141)	0.13	0.18	0.12	0.14	0.10	0.13	0.08	0.15	0.13
Sr (88)	136.51	107.68	216.03	157.46	135.12	127.49	227.12	162.51	225.70
Nd (146)	1.36	1.75	1.27	1.51	1.08	1.34	0.98	1.53	1.25
Zr (91)	21.39	24.71	20.98	21.80	20.39	20.86	20.33	22.30	18.47
Hf (177)	0.51	0.62	0.49	0.53	0.45	0.52	0.42	0.58	0.45
Sm (147)	0.53	0.74	0.48	0.64	0.41	0.53	0.33	0.63	0.49
Eu (151)	0.38	0.45	0.33	0.40	0.32	0.38	0.28	0.41	0.36
Gd (157)	1.92	2.23	1.84	2.07	1.76	1.91	1.74	2.03	1.69
Tb (159)	0.26	0.33	0.25	0.30	0.23	0.26	0.22	0.29	0.24
Dy (163)	1.18	1.67	1.07	1.46	0.93	1.19	0.77	1.38	1.08
Ho (165)	0.24	0.35	0.22	0.31	0.19	0.25	0.16	0.29	0.23
Y (89)	6.56	9.21	5.92	8.14	5.95	6.26	4.49	7.12	5.38
Er (167)	0.57	0.86	0.50	0.75	0.43	0.57	0.33	0.70	0.53
Tm (169)	0.07	0.11	0.06	0.09	0.05	0.07	0.03	0.09	0.06
Yb (174)	0.46	0.70	0.40	0.61	0.34	0.46	0.25	0.57	0.43
Lu (175)	0.05	0.09	0.04	0.07	0.03	0.05	0.02	0.07	0.05
Ni (58)	132.95	148.83	94.52	103.89	215.04	125.55	127.73	65.05	98.37

Unit: ppm

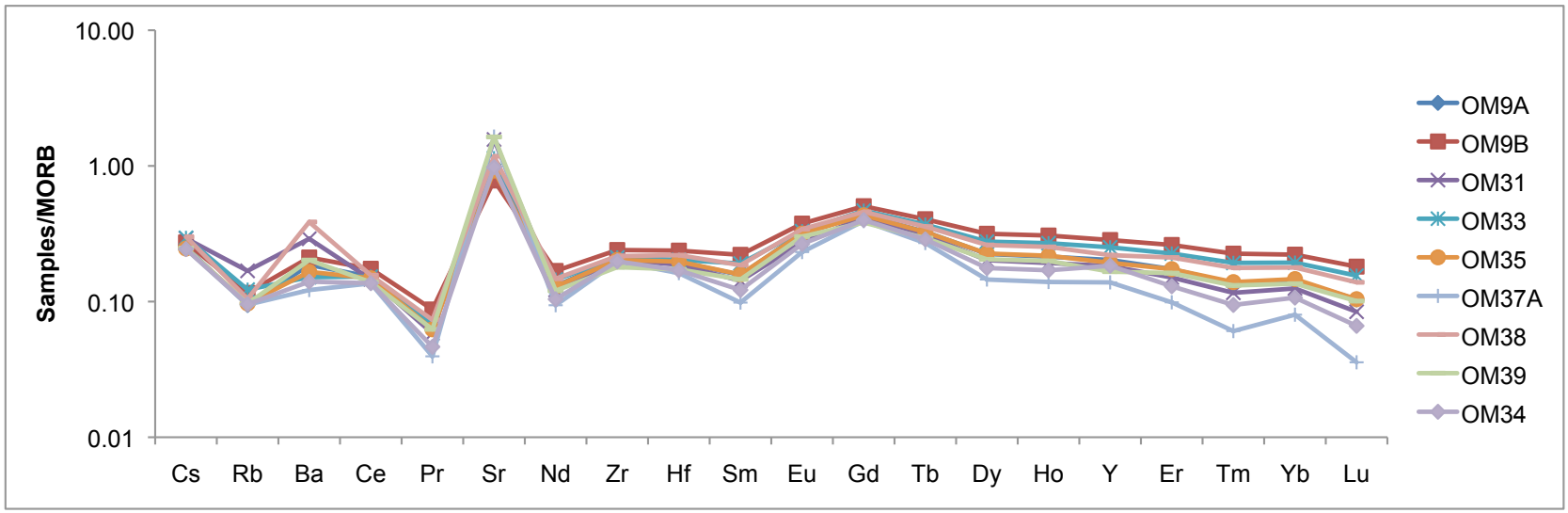

Figure 8. MORB normalized spider diagram of trace element data for samples from the outcrop of lower gabbro in Sumail nappe. Sr concentration in the samples is near the MORB value, while the rest trace elements are depleted.

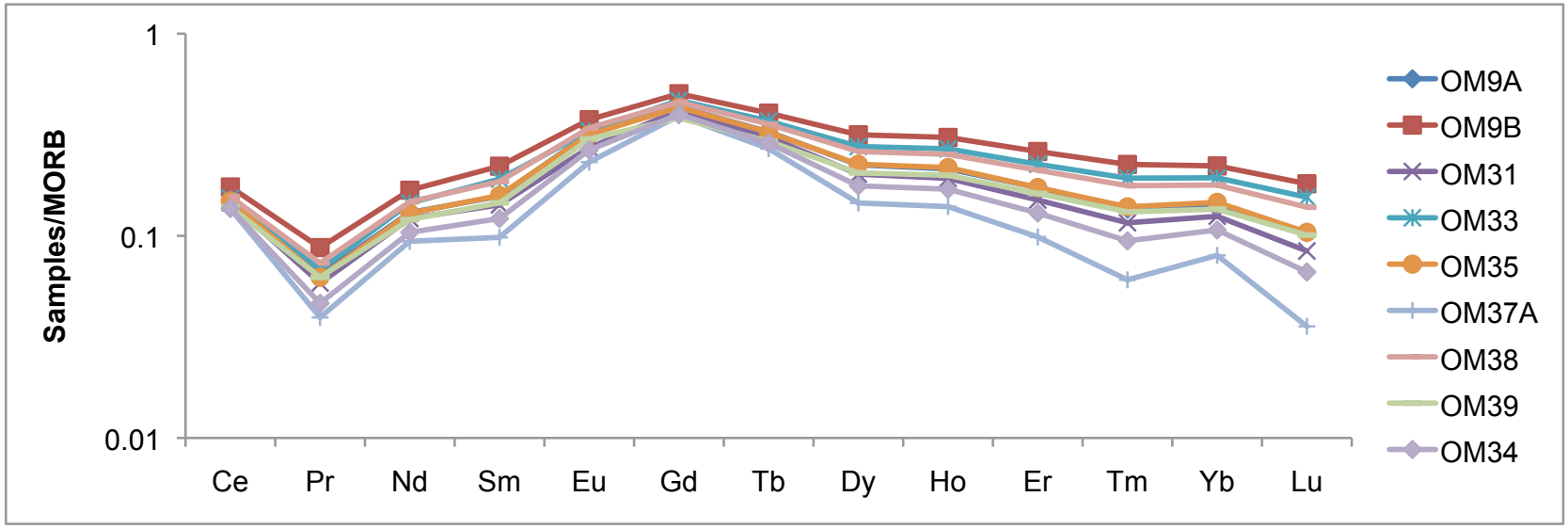

Figure 9. MORB normalized spider diagram of rare earth elements (REE) for samples from the outcrop of lower gabbro in Sumail nappe. All sample have been depleted in REE, compared to MORB.

Table 7. $^{87}Sr/^{86}Sr$ and $\delta^{18}O$ of sampled Oman ophiolite. Replica $\delta^{18}O$ analyses are reported.

Sample Name	$^{87}Sr/^{86}Sr$	2σ	$\delta^{18}O$	
Upper Gabbro				Replica
OM45	0.70801	±1	2.50	2.30
OM46	0.70356	±1	4.43	
OM47	0.70321	±1	6.26	
OM48	0.70345	±1	5.30	
Middle Gabbro				
OM40	0.70410	±2	5.54	
OM40A	0.70445	±2	5.64	
OM40B			5.44	
OM15A	0.70407	±1	6.15	
OM15B	0.70308	±1	6.02	
OM16	0.70342	±1	5.32	
OM19	0.70595	±9	5.30	
Lower Gabbro				
OM9A			5.02	
OM9B	0.70328	±17	4.92	
OM31	0.70417	±2	5.00	
OM33	0.70458	±1	3.46	
OM34	0.70313	±2	5.78	6.14
OM35	0.70321	±1	6.46	
OM37A	0.70429	±6	4.21	
OM37B	0.70641	±1	4.08	
OM38	0.70368	±1	5.37	
OM39	0.70409	±3	6.07	
OM28	0.70385	±1	6.74	
Moho				
OM49	0.70855	±1	4.84	5.41
OM49A	0.70352	±2	6.13	
OM49B			4.33	
OM50	0.70517	±1	4.06	
MTZ				
OM7	0.70855	±2	9.90	10.30
OM8	0.70850	±1	30.20	30.90
OM8A	0.70840	±2	7.14	
OM8C	0.70847	±2	28.50	28.70
OM8E	0.70375	±1	6.15	
OM8F-1	0.70721	±1	4.71	
OM8F-2	0.70640	±1	7.60	8.00
OM8G	0.70412	±1	3.30	2.60
OM8H	0.70406	±1	7.56	

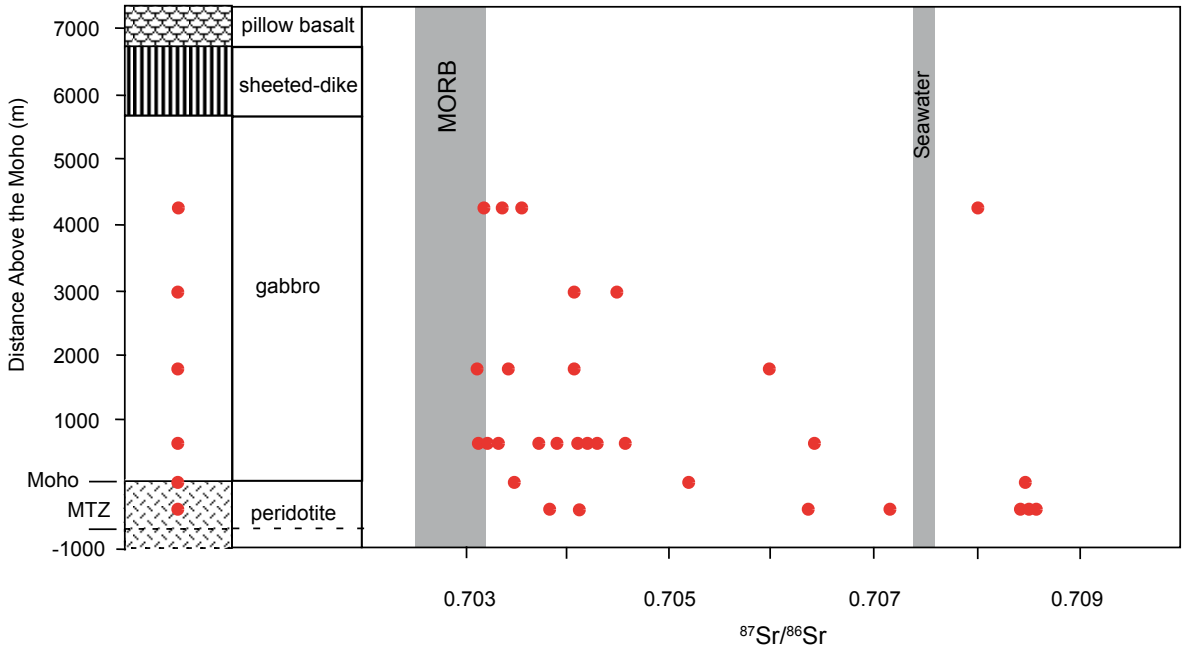

Figure 10. Variation of $^{87}Sr/^{86}Sr$ composition as a function of the depth of the studied samples of the Oman ophiolite. Thickness of each section is from Bosch *et al*. (2004). The field for MORB is from White and Klein (2011, in press) and the field for seawater is from McArthur *et al* (2001). Red dots in schematic log show samples depth relative to Moho.

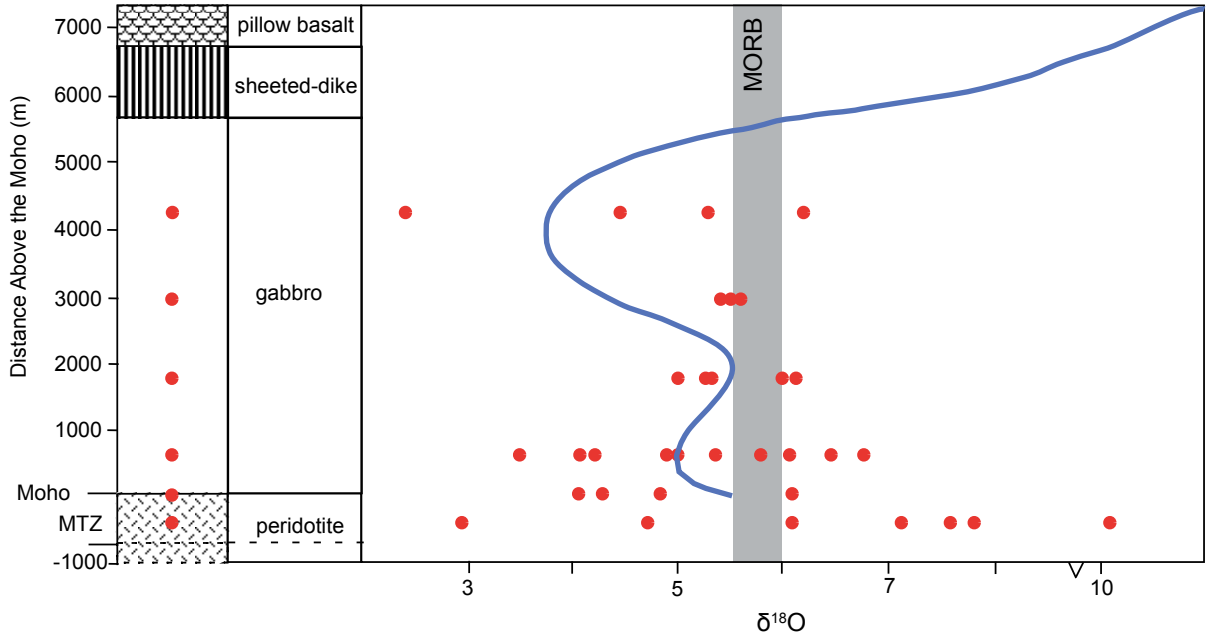

Figure 11. Variation of $\delta^{18}O$ as a function of the location of the studied samples in the crustal section of the Oman ophiolite. The field for MORB is from White and Klein (2011, in press). Blue curve corresponds to the whole rock data from Gregory & Taylor (1981).

from the depth of the Moho and Moho Transition Zone, and the other one is from the upper gabbro section. Two samples from MTZ (OM8 and OM8C) are magnesite rocks ($MgCO_3$) with $\delta^{18}O$ ~30 and are of obvious secondary origin. Two serpentinite samples (OM7 and OM8A) from MTZ have $\delta^{18}O$ of 10.10 and 7.14 respectively. The peridotite from the Moho has $\delta^{18}O$ of 4.84 and the sample from the upper gabbro has $\delta^{18}O$ of 2.40. For the samples with $^{87}Sr/^{86}Sr$ ratios $\geq$ 0.7074, leaching experiment results are in Table 8. For OM7, OM8A and OM49, leached and unleached $^{87}Sr/^{86}Sr$ ratios are identical within analytical error. The $^{87}Sr/^{86}Sr$ value of OM45, however, decreases from 0.70801 to 0.70701 after leaching.

Table 8. Leaching experiments on samples with $^{87}Sr/^{86}Sr$ larger than 0.7074, which is Cretaceous seawater value at 95 Ma.

Sample	Locality	Description	Distance to Moho	$^{87}Sr/^{86}Sr$	$\delta^{18}O$
OM-45	Wadi-Tayin	gabbro	4.2 km	0.70801	2.40
solid				0.70701	
leachate				0.70824	
OM-49	Nakhl	peridotite	Moho	0.70855	4.84
solid				0.70858	
leachate				0.70864	
OM-7	Sumail	altered dunite	MTZ	0.70855	10.10
solid				0.70853	
leachate				0.70855	
OM-8A	Sumail	altered dunite	MTZ	0.70840	7.14
solid				0.70839	
leachate				0.70856	

METASOMATIC ANALYSIS

Principle

Most of the rocks analyzed in this study show obvious signs of hydrothermal alteration; they have likely undergone metasomatism, i.e., change in composition through reaction with a fluid. Metasomatism analysis attempts to quantify this change and requires knowledge of the chemical compositions of the altered rock and its precursor. While the chemical compositions of the altered rocks can be measured, determining that of the precursor rock is more difficult, especially when the metasomatism is pervasive as is the case in this study. One must rely on the freshest samples available. Thin section examination and Sr and O isotope ratios were the primary criteria used to determine which samples have experienced the least metasomatic change: those samples with the greatest proportion of primary igneous minerals (plagioclase and clinopyroxene for gabbro) and $^{87}Sr/^{86}Sr$ ratios and $\delta^{18}O$ values closest to MORB values (0.7029 and 5.69, respectively) were deemed freshest in this study.

Immobile elements can be used to quantify a rock's mass and volume change as well as enrichment or depletion of more mobile elements. The principle is that the absolute amount of immobile elements does not change, no matter how much mass/volume loss/gain has occurred. However, the concentration of immobile elements may change due to the change of mass/volume. From the concentration change of immobile elements, the rock mass change can be calculated, as described

below. While no elements are completely immune from metasomatic change, "immobile elements", that is, elements with low solubilities in aqueous fluids, typically experience far less change than other elements. Immobile elements are typically metals with valence states of +3 to +5 and include Al, the high field strength elements (Hf, Zr, Nb, Ta), and the rare earth elements. Once the original rock and the immobile elements are identified, it is straightforward to derive the necessary mass balance equations. The following section of equations for mass change, volume change and element concentration change is from book "Principles of igneous and metamorphic petrology" by Philpotts and Ague (2009). Phipotts and Ague's method is based on the work of Gresens (1967), Grant (1986), Brimhall & Dietrick (1987), Ague (1994), and Ague & van Haren (1996).

Mathematics

Mass balance for an immobile element i, may be expressed as:

$$V^o \rho^o c_i^o = V' \rho' c_i' \qquad (1)$$

where V is the rock volume, ρ is bulk rock density, c_i is the concentration of a perfectly immobile element i, and the superscripts ^{o} and $'$ refer to original and altered rock, respectively. Equation (1) states that the mass of i in the altered rock and that of the original are the same. The total rock mass is given by the product of volume and density. Thus, the change in total rock mass, T_{mass} can be written as

$$T_{mass} = \frac{V' \rho' - V^o \rho^o}{V^o \rho^o} \qquad (2)$$

Rearranging equation (1) gives:

$$V^o\rho^o = V'\rho'\frac{c_i'}{c_i^o} \tag{3}$$

Substitution of equation (3) into equation (2) and rearranging gives [Ague, 1994]

$$T_{mass,i} = \frac{c_i^o}{c_i'} - 1 \tag{4}$$

where $T_{mass,i}$ is the total rock mass change calculated based on immobile element i. $T_{mass,i}$ is a fraction; the percentage mass change can be found by multiplying by 100. Negative $T_{mass,i}$ means the loss of mass in the altered rock, and positive $T_{mass,i}$ means the gain of mass in the altered rock. From equation (4), the rock mass change can be calculated from the concentration of the immobile element in the original rock and the altered rock.

Concentrations of mobile elements can vary for reasons other than rock mass change. Quantifying these variations may be useful in understanding the processes that produced them. If the conditions of temperature and pressure for each sample could be recognized from the assemblage of minerals, the systematic gain/loss of different elements under different conditions of temperature and pressure would be clear. The change in mass for any mobile element j can be defined as

$$\tau^j = \frac{V'\rho'c_j' - V^o\rho^o c_j^o}{V^o\rho^o c_j^o} \tag{5}$$

where τ^j is the fractional change in mass of mobile element j.

In the above equation, there are several physical properties of rock that need to be measured to get the mass change for any mobile element. If a simpler version only involving concentration can be derived, efforts would be saved in analysis. A

simpler equation for each element's mass change may be derived from the volume change as follows:

If volume change is defined as

$$\varepsilon = \frac{V' - V^o}{V^o} \tag{6}$$

Rearranging equation (1) gives

$$V' = \frac{V^o \rho^o c_i^o}{\rho' c_i'} \tag{7}$$

Substituting (7) into (6) and rearranging gives:

$$\varepsilon_i = (\frac{c_i^o}{c_i'})(\frac{\rho^o}{\rho'}) - 1 \tag{8}$$

If the density of original rock (ρ') and altered rock (ρ^o) are measured, the volume change of each altered rock can be calculated using equation (8).

To eliminate the volume terms in equation (5), rearrange equation (6) into

$$\frac{V'}{V^o} = \varepsilon_i + 1 \tag{9}$$

Substituting (9) into (5) yields

$$\tau_i^j = (\frac{c_j'}{c_j^o})(\frac{\rho'}{\rho^o})(\varepsilon_i + 1) - 1 \tag{10}$$

To eliminate the density terms, substituting (8) into (10) yields

$$\tau_i^j = (\frac{c_i^o}{c_i'})(\frac{c_j'}{c_j^o}) - 1 \tag{11}$$

From equation (11), if the concentration ratio of immobile element *i* in original rock/altered rock and the concentration ratio of mobile element *j* in altered

rock/original rock are known, the mass change for any individual mobile species can be calculated. All these expressions are concentration ratios because the use of ratios cancels out the 100% normalization inherent in all weight percent data.

Analysis Results

The cross-section in Wadi Samarh from the Sumail nappe was selected for metasomatism analysis. The samples were about 0.6 km above Moho in the crustal section of the Oman ophiolite. According to the structural mapping conducted by Nicolas and Boudier (2000), the gabbro section at Sumail nappe is ~2 km thick, much thinner than the composite thickness (5.7 km) in Figure 10 & 11. Samples OM37A, OM38 and OM39 that are from nearby outcrops are also included in metasomatism analysis. However, only OM9A, OM9B, OM31, OM34 and OM35 have the same starting compositions because they were sampled within 10 m of vertical distance. Gabbros OM33, OM37A, OM38 and OM39 are assumed to have similar starting compositions as the above four gabbros, but might not be exactly the same. From thin section observations, OM33 has finer grain sizes. OM37A has larger grains and less oriented. OM38 and OM39 also have larger size of grains.

OM34 was chosen as precursor rock to which the altered rocks were compared based on its nearly MORB-like $^{87}Sr/^{86}Sr$ (0.7031) and $\delta^{18}O$ (5.78) and the observation of very little alteration in thin section. Zr, a high field strength element, and Gd, a rare earth element, were chosen as immobile elements in this analysis as the Zr/Gd is nearly constant (11.14±0.36) across the entire set of samples. Mass changes of samples calculated using equation (4) are summarized in Table 9. $\delta^{18}O$

Table 9. Summarization of mass changes for samples from lower gabbro section in Sumail nappe. Calculations are based on immobile elements Gd and Zr, respectively. $\delta^{18}O$ data are reported to indicate the alteration temperature. The equation that is used to calculate mass change is equation (4).

Samples	Gd	Zr	Gain/Loss	$\delta^{18}O$	T
OM9A	-0.08	-0.05	Loss	5.02	high
OM9B	-0.21	-0.17	Loss	4.92	high
OM31	-0.04	-0.03	Loss	5.00	high
OM33	-0.15	-0.06	Loss	3.46	high
OM35	-0.08	-0.02	Loss	6.46	low
OM37A	0.02	0.00	Gain	4.21	high
OM38	-0.13	-0.09	Loss	5.37	high
OM39	0.04	0.10	Gain	6.07	low

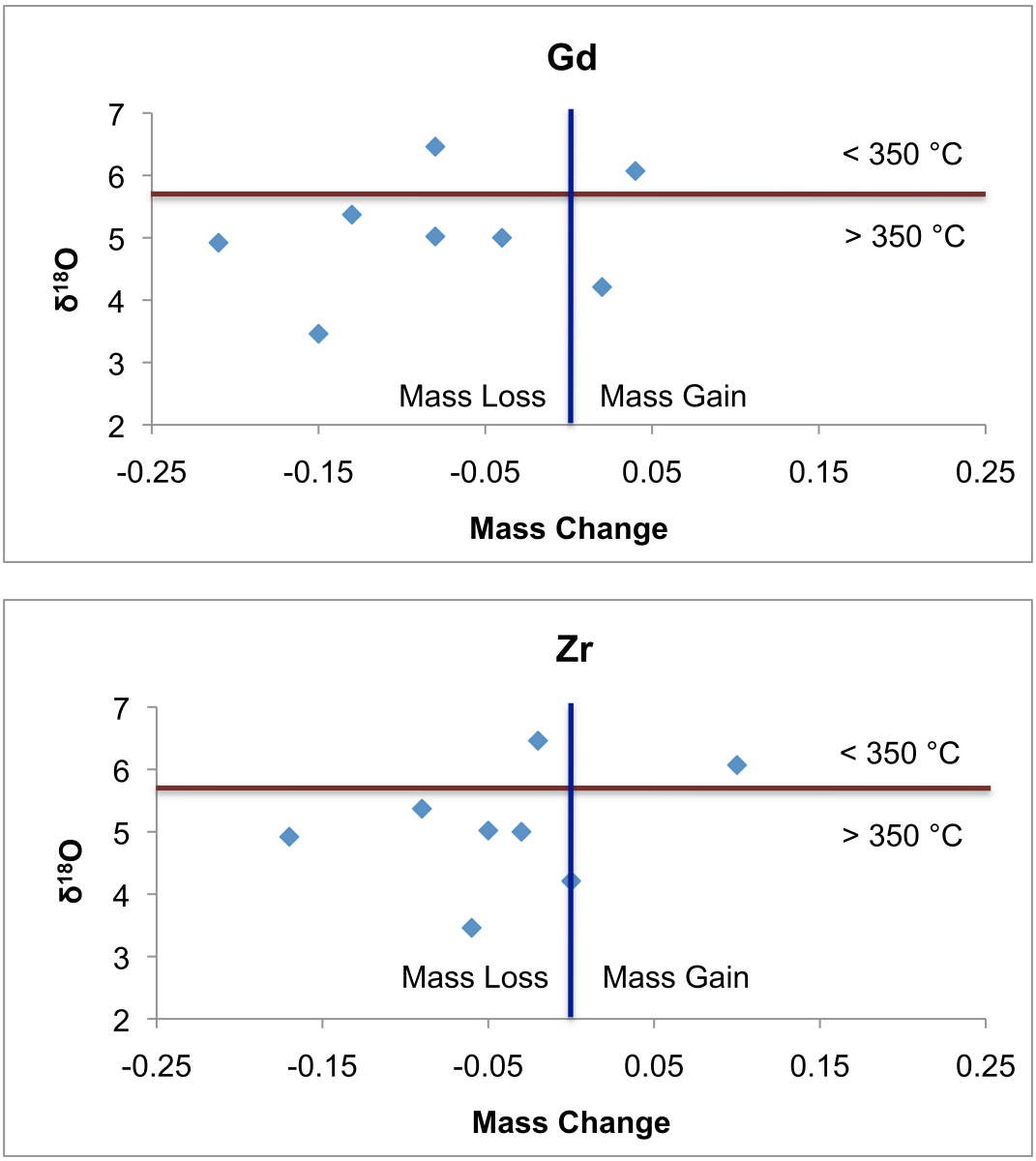

Figure 12. Plots of mass changes of altered rocks and $\delta^{18}O$ values. Mass changes are calculated using Gd and Zr as the immobile element, respectively. $\delta^{18}O$ is the indicator of alteration temperature. Alteration occurs below 350 °C for rocks with $\delta^{18}O$ bigger than 5.69, and alteration is above 350 °C for rocks with $\delta^{18}O$ smaller than 5.69.

values and mass changes based on immobile element Zr and Gd are plotted in Figure 12, respectively. OM37A and OM39 experienced mass gain, while the rest of the gabbros lost mass during metasomatism.

Quantitatively, the enrichment or depletion of each element is worthy of note if the alteration temperature can be obtained. Figure 13 shows the concentration ratios of each element in altered rock/original rock for each altered rock. The dash lines in every figure of Figure 13 are horizontal lines connecting the two immobile elements: Zr and Gd. As a result, the dash lines define the elements that don't experience mass changes. The elements that fall above the dash lines have been enriched in the altered samples, while the elements that fall below the dash lines have been depleted in the altered samples. Appendix 1 summarizes the ratios that are plotted in Figure 13. Table 10 shows the main element gain/loss for each sample, and Table 11 summarizes how much percentage change happens for each element calculated from Zr and Gd respectively. There are some discrepancies between the elemental mass change calculated from immobile element Zr and that calculated from immobile element Gd (labeled in red). However, most results agree very well, which indicates choosing Zr and Gd as immobile elements is wise. Figure 13(a) shows the element enrichment or depletion of samples from the big outcrop in Wadi Samarh except OM31. Figure 13(b) presents element change of two samples, OM33 that is from the same outcrop but not the same layer of rocks and OM31 that has veins of epidote. Figure 13(c) plots the enrichment and depletion of OM37A, .

Table 10. Element gain/loss of samples from Wadi Samarh in Sumail nappe. $\delta^{18}O$ data are reported to indicate the alteration temperature.

Sample	Depletion	Enrichment	$\delta^{18}O$	T	$^{87}Sr/^{86}Sr$
OM9A	Cs, Rb, Sr, major elements except P	REE, Ba, P	5.02	high	
OM9B	Sr, major elements	REE, Y, Ba	4.92	high	0.7033
OM31	major elements except Al, Ca	Al, Ba, REE, Sr, Rb	5.00	high	0.7042
OM33	major elements except P	Al, Cs, Rb, Ba, Sr, REE, Y	3.46	high	0.7046
OM35	Al, Fe, Mg, Na, Cs, Rb, Sr	Mn, Ca, P, Ba, REE	6.46	low	0.7032
OM37A	Fe, Mn, Mg, Ba, REE, Y	Si, Al, Na, Sr, P, Sr	4.21	high	0.7043
OM38	major elements except Na	REE, Na, Cs, Ba	5.37	high	0.7037
OM39	Fe, Mn, Mg	Al, Na, P, Cs, Rb, Ba, REE, Sr	6.07	low	0.7041

Table 11. Mass change of each element for samples from the lower gabbro section. Calculations are conducted using Zr and Gd as immobile element respectively. There are discrepancies between the elemental mass change calculated from immobile element Zr and that calculated from immobile element Gd (different signs of mass change are labeled in red). However, most results agree well. The equation that is used to calculate the elemental mass change is equation (11).

	OM9A/OM34		OM9B/OM34		OM31/OM34		OM33/OM34		OM35/OM34		OM37A/OM34		OM38/OM34		OM39/OM34	
	Zr	Gd	Zr	Gd	Zr	Gd	Zr	Gd	Zr	Gd	Zr	Gd	Zr	Gd	Zr	Gd
SiO_2	-0.02	-0.06	-0.14	-0.18	-0.03	-0.04	-0.03	-0.12	0.00	-0.06	0.01	0.03	-0.16	-0.21	0.01	-0.05
Al_2O_3	-0.03	-0.07	-0.28	-0.31	0.21	0.19	-0.07	-0.16	-0.04	-0.09	0.19	0.21	-0.21	-0.25	0.22	0.15
FeO	-0.15	-0.18	-0.28	-0.31	-0.41	-0.42	-0.28	-0.34	-0.05	-0.10	-0.36	-0.35	0.02	-0.03	-0.46	-0.49
MnO	0.02	-0.02	-0.20	-0.23	-0.25	-0.26	-0.29	-0.35	0.13	0.06	-0.23	-0.22	-0.19	-0.23	-0.45	-0.48
MgO	-0.09	-0.13	-0.21	-0.24	-0.31	-0.32	-0.13	-0.21	-0.02	-0.08	-0.15	-0.13	-0.25	-0.29	-0.30	-0.33
CaO	0.00	-0.03	-0.07	-0.11	0.07	0.05	0.02	-0.07	0.06	0.00	0.08	0.09	-0.18	-0.22	0.00	-0.05
Na_2O	0.03	-0.01	-0.25	-0.28	-0.10	-0.11	-0.13	-0.21	-0.13	-0.18	0.14	0.15	0.09	0.04	0.81	0.71
P_2O_5	0.08	0.04	0.05	0.00	0.01	-0.01	0.16	0.06	0.07	0.01	0.07	0.09	-0.22	-0.25	0.35	0.28
Cs	-0.01	-0.05	-0.07	-0.11	0.17	0.15	0.13	0.03	-0.01	-0.07	0.01	0.02	0.13	0.07	0.12	0.06
Rb	-0.06	-0.09	0.00	-0.04	0.71	0.69	0.20	0.09	-0.01	-0.06	0.00	0.01	0.00	-0.05	0.12	0.05
Ba	0.27	0.22	0.24	0.19	1.01	0.98	0.01	-0.08	0.15	0.09	-0.13	-0.12	1.52	1.39	0.59	0.50
Ce	0.06	0.02	0.05	0.01	0.04	0.02	0.05	-0.05	0.06	0.00	0.00	0.01	0.05	0.00	0.12	0.06
Pr	0.32	0.27	0.56	0.49	0.22	0.21	0.37	0.25	0.32	0.24	-0.15	-0.14	0.44	0.37	0.49	0.40
Sr	-0.04	-0.07	-0.34	-0.37	0.55	0.53	0.09	-0.01	-0.08	-0.13	0.69	0.71	0.10	0.05	0.84	0.74
Nd	0.19	0.15	0.33	0.28	0.14	0.12	0.31	0.19	0.21	0.15	-0.09	-0.08	0.29	0.23	0.28	0.21
Zr	0.00	-0.04	0.00	-0.04	0.00	-0.01	0.00	-0.09	0.00	-0.06	0.00	0.01	0.00	-0.05	0.00	-0.06
Hf	0.10	0.06	0.15	0.10	0.07	0.05	0.12	0.02	0.13	0.07	-0.04	-0.03	0.18	0.12	0.12	0.06
Sm	0.23	0.19	0.50	0.43	0.14	0.12	0.47	0.34	0.27	0.20	-0.19	-0.18	0.39	0.33	0.32	0.25
Eu	0.15	0.11	0.17	0.12	0.00	-0.02	0.16	0.06	0.16	0.10	-0.13	-0.11	0.18	0.12	0.25	0.18
Gd	0.04	0.00	0.04	0.00	0.01	0.00	0.10	0.00	0.06	0.00	-0.01	0.00	0.05	0.00	0.06	0.00
Tb	0.08	0.04	0.16	0.11	0.04	0.03	0.20	0.10	0.11	0.04	-0.06	-0.05	0.14	0.08	0.13	0.07
Dy	0.21	0.17	0.48	0.41	0.11	0.09	0.46	0.33	0.25	0.18	-0.17	-0.16	0.35	0.29	0.28	0.21
Ho	0.20	0.16	0.49	0.43	0.10	0.08	0.48	0.35	0.25	0.18	-0.18	-0.17	0.36	0.29	0.29	0.22
Y	0.05	0.01	0.28	0.22	-0.03	-0.05	0.28	0.17	0.03	-0.03	-0.24	-0.23	0.09	0.04	0.00	-0.06
Er	0.28	0.23	0.66	0.59	0.13	0.11	0.63	0.49	0.31	0.23	-0.24	-0.23	0.49	0.42	0.38	0.30
Tm	0.37	0.32	0.97	0.89	0.19	0.18	0.91	0.74	0.44	0.36	-0.36	-0.35	0.71	0.63	0.54	0.45
Yb	0.28	0.23	0.71	0.64	0.14	0.12	0.69	0.54	0.34	0.26	-0.25	-0.24	0.52	0.45	0.40	0.32
Lu	0.49	0.44	1.26	1.16	0.24	0.22	1.19	1.00	0.54	0.45	-0.46	-0.45	0.92	0.82	0.68	0.59

Figure 13. (a) Depletion and enrichment diagram of OM9A, OM9B and OM35 relative to OM34. Black dash lines are "line of elements with no mass change" defined by immobile elements Zr and Gd. Elements that fall above the line are enriched in samples, and elements that fall below the line are depleted in samples, compared to original rock OM34. Plotted samples have similar trace element pattern. (b) Depletion and enrichment diagram of OM33 and OM31 from the same outcrop in Wadi Samarh. OM33 is from the same outcrop, but not in the same layer as OM34. OM31 has veins of epidote and is from the same layer as OM34. (c) Depletion and enrichment diagram of OM37A, OM39 and OM38 that are from nearby outcrops.

Figure 13. (a)

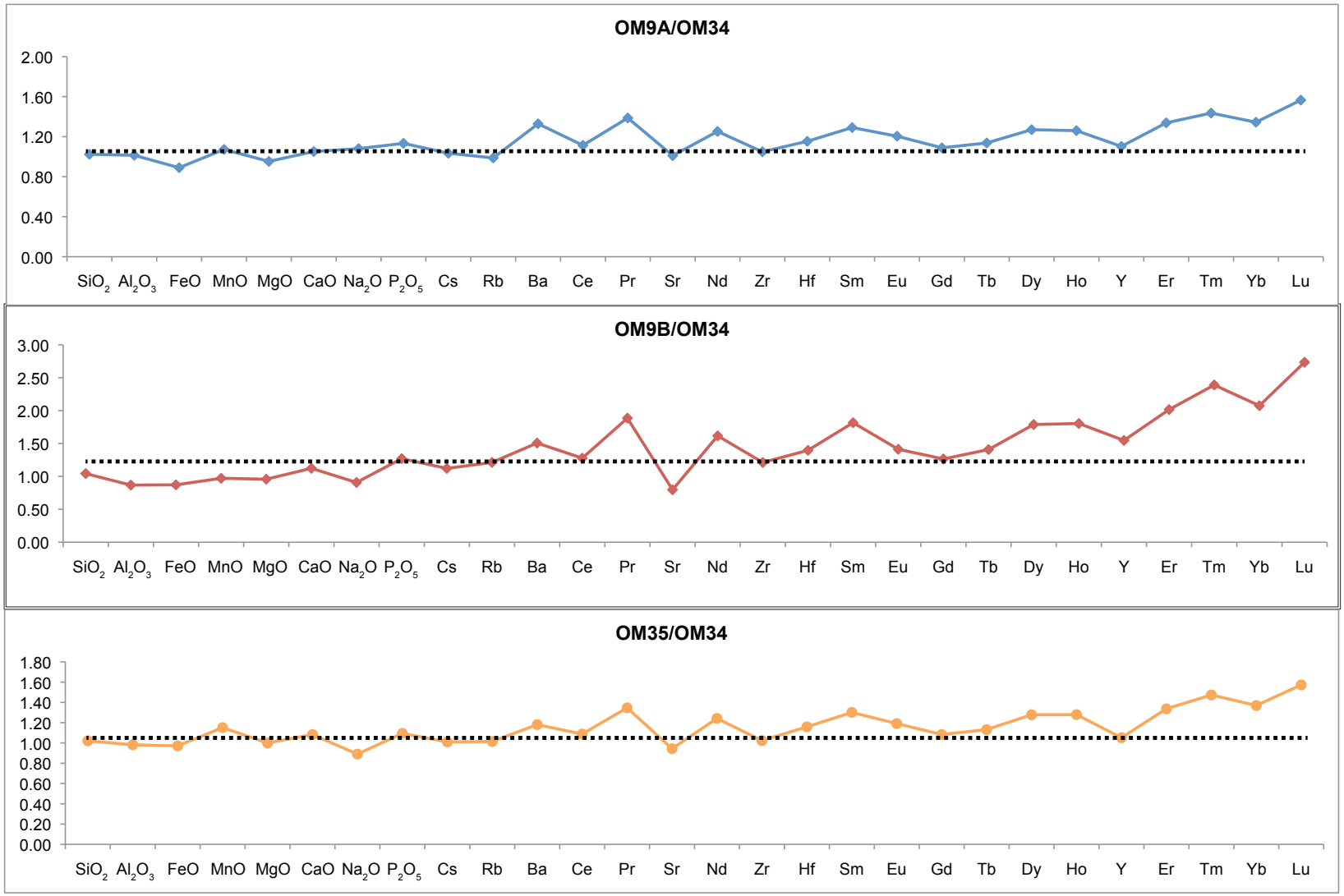
OM9A/OM34
2.00
1.60
1.20
0.80
0.40
0.00
SiO2 Al2O3 FeO MnO MgO CaO Na2O P2O5 Cs Rb Ba Ce Pr Sr Nd Zr Hf Sm Eu Gd Tb Dy Ho Y Er Tm Yb Lu
OM9B/OM34
3.00
2.50
2.00
1.50
1.00
0.50
0.00
SiO2 Al2O3 FeO MnO MgO CaO Na2O P2O5 Cs Rb Ba Ce Pr Sr Nd Zr Hf Sm Eu Gd Tb Dy Ho Y Er Tm Yb Lu
OM35/OM34
1.80
1.60
1.40
1.20
1.00
0.80
0.60
0.40
0.20
0.00
SiO2 Al2O3 FeO MnO MgO CaO Na2O P2O5 Cs Rb Ba Ce Pr Sr Nd Zr Hf Sm Eu Gd Tb Dy Ho Y Er Tm Yb Lu

Figure 13 (b)

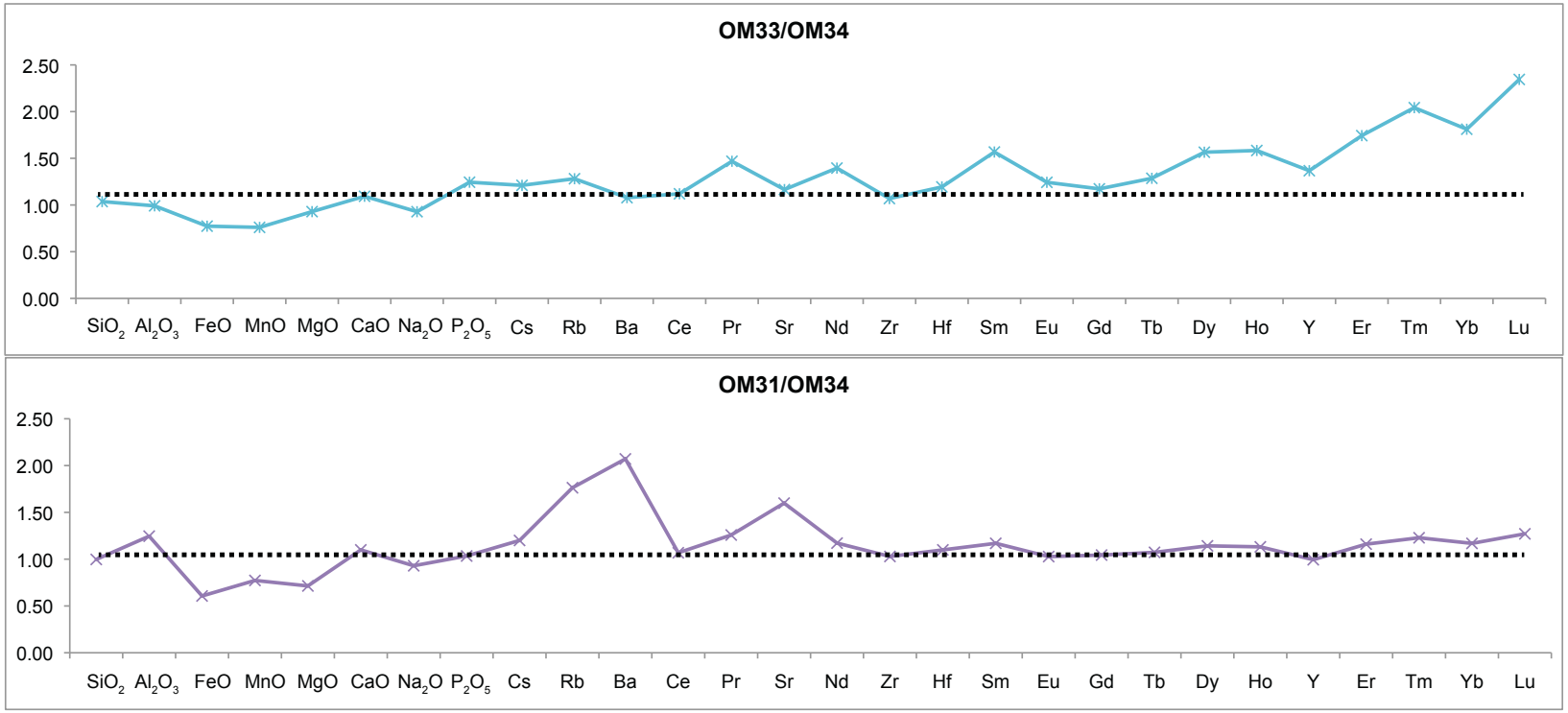
OM33/OM34
2.50
2.00
1.50
1.00
0.50
0.00
SiO2 Al2O3 FeO MnO MgO CaO Na2O P2O5 Cs Rb Ba Ce Pr Sr Nd Zr Hf Sm Eu Gd Tb Dy Ho Y Er Tm Yb Lu
OM31/OM34
2.50
2.00
1.50
1.00
0.50
0.00
SiO2 Al2O3 FeO MnO MgO CaO Na2O P2O5 Cs Rb Ba Ce Pr Sr Nd Zr Hf Sm Eu Gd Tb Dy Ho Y Er Tm Yb Lu

Figure 13 (c)

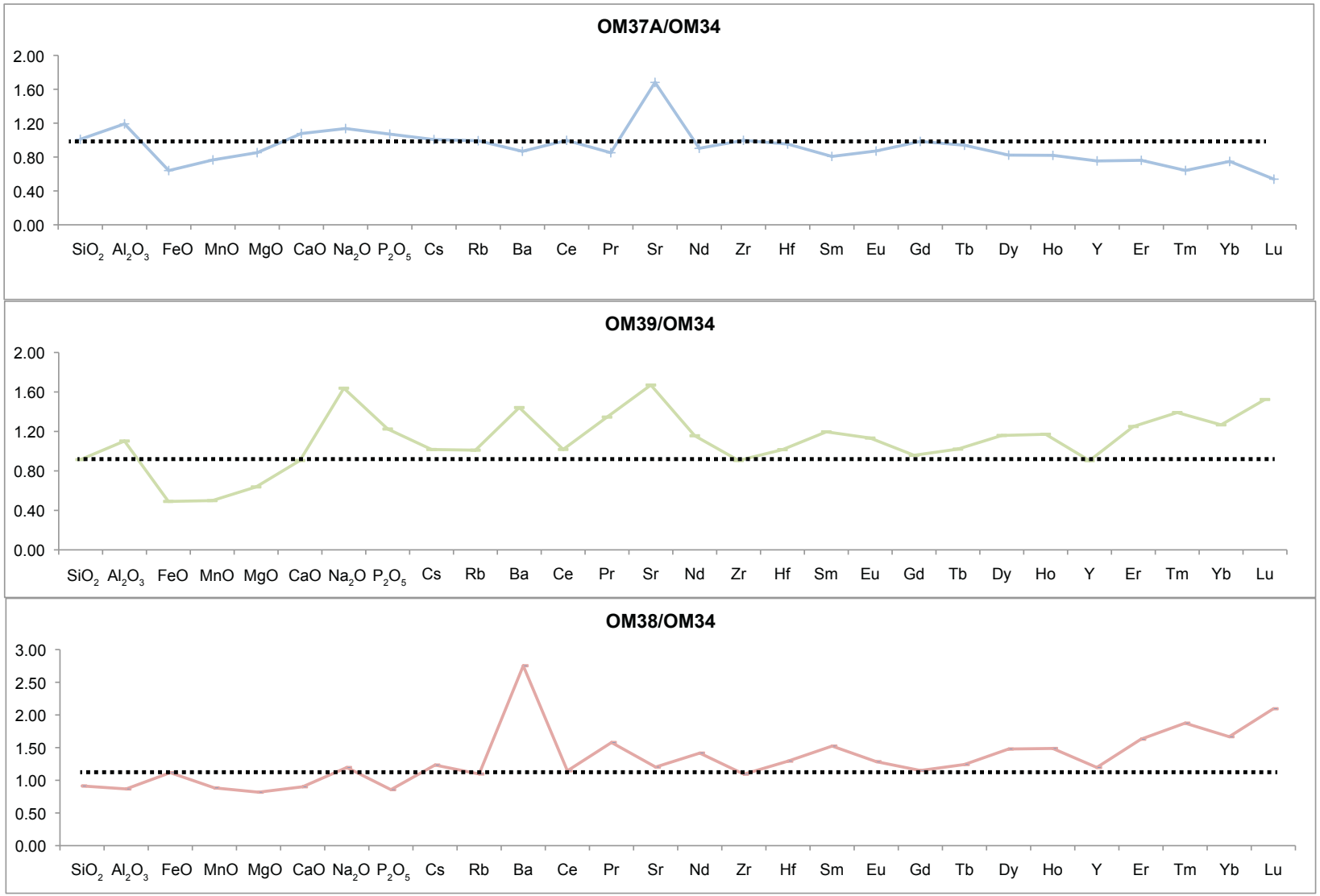
OM37A/OM34
2.00
1.60
1.20
0.80
0.40
0.00
SiO2 Al2O3 FeO MnO MgO CaO Na2O P2O5 Cs Rb Ba Ce Pr Sr Nd Zr Hf Sm Eu Gd Tb Dy Ho Y Er Tm Yb Lu
OM39/OM34
2.00
1.60
1.20
0.80
0.40
0.00
SiO2 Al2O3 FeO MnO MgO CaO Na2O P2O5 Cs Rb Ba Ce Pr Sr Nd Zr Hf Sm Eu Gd Tb Dy Ho Y Er Tm Yb Lu
OM38/OM34
3.00
2.50
2.00
1.50
1.00
0.50
0.00
SiO2 Al2O3 FeO MnO MgO CaO Na2O P2O5 Cs Rb Ba Ce Pr Sr Nd Zr Hf Sm Eu Gd Tb Dy Ho Y Er Tm Yb Lu

OM38 and OM39, which are from nearby outcrop in the same wadi.

Thin section study of the gabbros shows that they have similar rock forming minerals. Plagioclase is the most abundant minerals in all thin sections, which is about 50 ~ 60% by volume percentage. Clinopyroxene is about 25 ~ 30%, and olivine 5 ~ 10%. Alteration minerals include serpentine, chlorite, hornblende, anthophyllite, opaque oxide, epidote and quartz. OM33 has a finer grain size compared to the rest of the samples. OM31 has veins of epidote and OM39 has a vein filled with quartz. The minerals filling the veins are alteration products, but they will affect the result of metasomatism analysis. The reason is that the process is not hydrothermal fluid exchanging elements with gabbros; instead, it is depositing/adding entirely new rock in the system. OM37A doesn't have veins, but the rock is fractured.

OM9A experienced extensive serpentinization and lost 5 ~ 8% of its mass during alteration. OM9A has been depleted in major elements. OM9B has a series of microcracks normal to the mineral lineation. It has been depleted in major elements and lost 17 ~ 21% of the mass. OM31 was sampled from highly fractured zones and has veins of epidote. OM31 lost 3 ~ 4% of the total mass and has been depleted in major elements except Al. OM34, our precursor rock, is very fresh and alteration happens mostly around olivine and clinopyroxene crystals. OM35 lost 2~8% of the mass and has been depleted in major elements except Ca. OM33, which has smaller mineral grain size compared to the other gabbros from the same outcrop, is highly altered and has abundant hornblende. The mass loss of OM33 is 6

~ 15%. OM38 experienced 9 ~ 13% mass loss, and the alteration minerals include hornblende, chlorite and serpentine. The samples that have lost mass are usually low in Al_2O_3 and CaO, which are about 35% in total by weight percentage. Elements Al and Ca go into plagioclase. One possibility is that these lower gabbros are relative rich in olivine and pyroxene, which are much more subject to breakdown and alteration than plagioclase. The exception is OM31 that is enriched in both Al_2O_3 and CaO, although it lost 3~4% of the mass. The epidote vein in OM31 can explain the enrichment of Al_2O_3 and CaO in this sample. The mass loss of OM31 might reflect hydrothermal dissolution of part of the rock.

Two samples that appear to have gained mass, OM37A (0 ~ 2% mass gain) and OM39 (4 ~ 10% mass gain), are rich in Al_2O_3 and Sr. These two elements are concentrated in plagioclase and, indeed, these samples are rich in normative plagioclase compared to OM34. Thus the enrichment of Al and Sr likely reflects the original rock composition rather than metasomatic gain. The quartz vein in OM39 could explain the apparent mass gain in this sample, although, curiously, OM39 shows no enrichment of SiO_2 in Figure 13.

Some of the apparent mobility of Al may simply reflect heterogeneity of the original rock compositions. Table 5 shows that normative mineral assemblages vary from rock to rock. OM31, OM37A and OM39, which are richer in Al_2O_3 and CaO do have higher normative plagioclase content. CIPW norms, of course, are ideal igneous minerals and do not necessarily reflect the real mineral assemblage. In the

case of OM31, the high normative plagioclase content may reflect the presence of epidote, a strictly metamorphic mineral, rather than igneous plagioclase.

DISCUSSIONS

Hydrothermal Alteration of the Oman ophiolite

As ocean floor spreads, cracks open in the oceanic lithosphere in response to the tensional stress. Seawater can percolate through this highly fractured and permeable lithosphere, driven by thermal gradients within the lithosphere, and react with it.

$\delta^{18}O$ is a measure of the ratio of stable isotopes ^{18}O and ^{16}O, and is calculated using the following equation:

$$\delta^{18}O = \frac{(^{18}O/^{16}O)_{sample} - (^{18}O/^{16}O)_{std}}{(^{18}O/^{16}O)_{std}} \times 1000$$

Standard Mean Ocean Water (SMOW) is the commonly used standard [Craig, 1961] for materials other than carbonates. From the equation above, a sample with $\delta^{18}O$ = 5 means that the sample is 5 per mil richer in ^{18}O than SMOW. Negative values indicate relative depletions of the heavy isotope in the samples compared to SMOW. Fresh unaltered basalts from mid-ocean ridge have average $\delta^{18}O$ of 5.69 ± 0.33 [White and Klein, 2011, in press]. The isotopic composition of the modern ocean is very uniform with a value of $\delta^{18}O$ = 0.

Whether the $\delta^{18}O$ of seawater was stable through Phanorozoic is controversial. Studies of carbonate fossils in 1960s and 1970s suggested that the $\delta^{18}O$ of ocean has been stable throughout the Mesozoic and Cenozoic [Taylor, 1974]. However, Veizer et al. (1999) presented data showing an increasing trending of $\delta^{18}O$

from −8‰ to 0‰ PDB (short for carbonate standard Pee Dee Belemnite) through Phanerozoic (570Ma-present) from measurements of brachiopods and belemnites, and a compilation of others' analyses. In their compilation, $\delta^{18}O$ values of planktonic forams at 95Ma are around −4‰ to −3.5‰. If the $\delta^{18}O$ measurements of carbonates that crystallize from seawater have changed overtime, $\delta^{18}O$ of seawater should have also changed through history. In contrast, Gregory and Taylor (1981), following Muehlenbachs (1976) argued that HT and LT hydrothermal alteration of the oceanic crust effectively buffered $\delta^{18}O$ of seawater in a way to keep its value close to 0‰. This argument was again made by Muehlenbachs *et al* (2003). My study focuses on the hydrothermal alteration processes and corresponding geochemical information. Hydrothermal alteration will increase or decrease $\delta^{18}O$ values of rocks under different temperature conditions. Regardless of whether $\delta^{18}O$ of seawater at 95Ma is 0‰ or −4‰, the overall result from seawater alteration is moving $\delta^{18}O$ of altered rocks away from 5.69 (fresh MORB value). The difference is the calculated amount of change based on different isotopic values of seawater. In my study, I am not using $\delta^{18}O$ values to quantify the amount of alteration. As a result, 0‰ is taken as the Cretaceous value of $\delta^{18}O$ following the value used by Bosch *et al* (2004).

The fractionation between ^{18}O and ^{16}O is temperature dependent. According to experimental and theoretical results, mineral-water fractionation factor (α) of many minerals has the trend of $\ln\alpha \propto \frac{1}{T^2}$[O'Neil and Taylor, 1967; O'Neil *et al.,* 1969; Wenner and Taylor, 1971, 1974]. At the temperature range of 300 ~ 400 °C, the net water-rock fractionation of oxygen isotope is small, <1-2 per mil. Thus, at or

above the temperature range of 300 ~ 400 °C, the isotopic exchange between seawater and oceanic crust will increase the $\delta^{18}O$ of seawater and decrease $\delta^{18}O$ of the oceanic crust. At low temperature or as seawater is cooled down when it rises up back to the surface, the oxygen isotope exchange will deplete ^{18}O seawater and enrich ^{18}O in oceanic crust, because the heavier isotope partitions into the solid phase.

However, the 350 ~ 400 °C maximum temperatures observed in hydrothermal vents on ocean floor make the alterations occurring above the 400°C questionable. Some suggested the rocks are effectively impermeable at high-temperature, and fluids cannot continue penetrating through rocks and thus rise to the surface and expel at the seafloor [Lister, 1974; Cathles, 1983; Fournier, 1991]. Others suggested the temperature cap is because of the thermodynamic properties of water. 20 ~ 30Mpa is a reasonable estimate of the pressure at the bottom of the ocean. The critical point of water is 374°C and 22MPa, in which 22MPa is a good estimate of pressure at ocean floor and 374 °C is similar to the maximum temperature of black smokers. Near the critical point, variations in properties of water tend to minimize viscous-drag force and maximize buoyancy forces [Ingebritsen and Hayba, 1994]. As a result, water rises and forms black smokers. However, the hydrothermal fluid can be above 350 ~ 400 °C within the crust. In contrast, drill samples from Hess Deep and exposed samples from the Oman ophiolites possessed amphibole-plagioclase pairs with calculated temperature above

700°C [Manning *et al.*, 2000]. Amphibole is a hydrous secondary mineral in the oceanic crust and it presence is indicative of H_2O fluids at this temperature.

$\delta^{18}O$ analyses of the gabbro section in this study show a wide range (red dots in Figure 11): upper gabbros: 2.30 ~ 6.26; middle gabbros: 5.30 ~ 6.15; lower gabbro, 3.46 ~ 6.74. The deviation of $\delta^{18}O$ from 5.69 (fresh MORB value) supports the conclusions of previous researchers that the entire crust section has been hydrothermally altered [Gregory & Taylor, 1981; Lanphere, 1981; McCulloch *et al.*, 1981; Bosch *et al.*, 2004]. Gregory and Taylor (1981) proposed a two-layer circulation system according to their whole rock $\delta^{18}O$ data. As shown from the blue curve in Figure 11, there is a low temperature circulation system within in the pillow lava and sheeted dike section, while below a thin sheet of impermeable magma, high temperature alteration (>500 °C) occurs within the gabbro section. Although there are not enough data in my analysis to summarize a systematic alteration trend with the increase of depth, $\delta^{18}O$, values from my study do not support the two-layer alteration model: upper, middle and lower gabbros all have $\delta^{18}O$ values inidicative of both high temperature (< 5.7) and low temperature alteration $\delta^{18}O$ values (> 5.7).

High temperature and low temperature alterations alternately swipe down to the Moho. The alterations in the oceanic lithosphere are controlled by fractures. The close correlation between fractures and alteration degree is robust in this study. The lower gabbros from Wadi Samarh in Sumail nappe sampled fresh rocks that are not affected by cracks and veins, altered rocks near fractures and rocks from highly

fractured zones. Figure 14 is the outcrop photo of the lower gabbro section with a histogram of frequency of the fractures. Samples that are not affected by cracks or veins have MORB isotopic values. For example, OM34 shows phase boundary migration under microscope, which is a characteristic magmatic process. OM34 also has $^{87}Sr/^{86}Sr$ of 0.7031 and $\delta^{18}O$ of 5.78. Samples that are affected by cracks or veins have elevated $^{87}Sr/^{86}Sr$ and deviated $\delta^{18}O$ values, for instance OM9B in Figure 14. Rocks that are sampled from fractures have obvious alteration isotopic values. In this study, OM31, which has altered isotopic values, was collected from very fractured zone and the thin section of this sample shows very strong alteration.

Using $\delta^{18}O$ values to categorize samples from the lower gabbro into HT alteration and LT alteration, there is no correlation between the gain/loss of rock mass and the alteration temperature (Table 9 and Figure 12). Six out of eight samples have lost mass in hydrothermal alteration. For each element's behavior, although the depletion of major elements and enrichment of REE are common feature in all samples from lower gabbro, there is no element that is exclusively depleted or enriched with by the alteration (Table 10). The depletion of major elements and the enrichment of REE are the result of rock mass lost during hydrothermal alteration.

Carbonation of the Oman Ophiolite

The Oman ophiolite is thought to represent a slice of Cretaceous lithosphere and obducted onto the Arabian platform during the late Cretaceous. Cretaceous

Figure 14. The outcrop of the lower gabbro section at Wadi Samarh in Sumail nappe, with labeled isotopic values. The histogram shows the frequency of fractures and veins from a 125-meter section (A − A'). The filled columns in the histogram represent highly fractured zones, and the unfilled columns represent less fractured zones. High frequency zones are light brown areas in the outcrop photo, and less fractured areas are dark brown color in the photo. Representative thin section images are taken from samples OM34, OM9B and OM31.

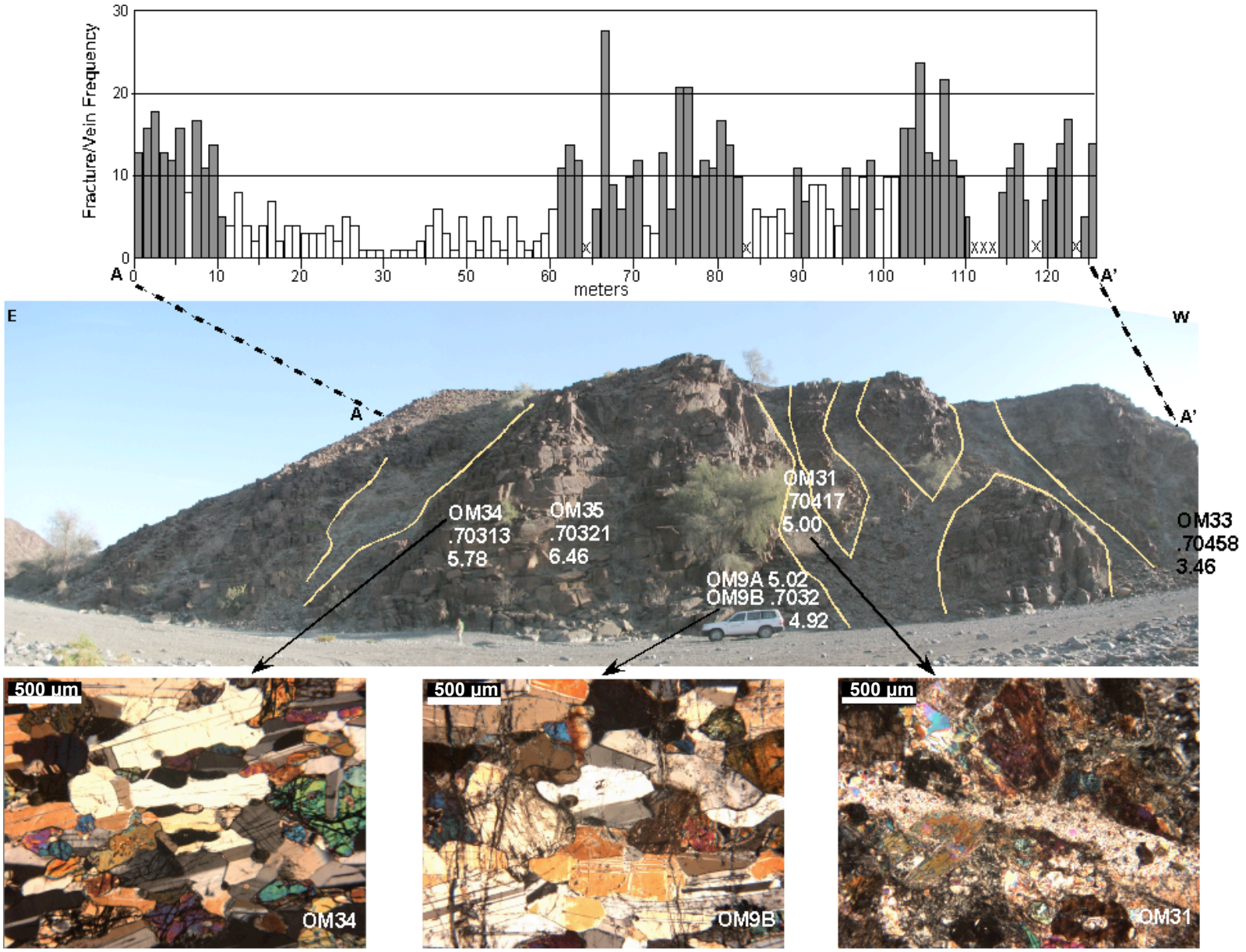
Fracture/Vein Frequency
30
20
10
0
A
0
10
20
30
50
60
70
80
90
100
110
120
meters
A'
E
W
A
A'
OM34
.70313
5.78
OM35
.70321
6.46
OM31
.70417
5.00
OM33
.70458
3.46
OM9A 5.02
OM9B .7032
4.92
500 µm
OM34
500 µm
OM9B
500 µm
OM31

seawater has $^{87}Sr/^{86}Sr$ of 0.7074 at 95 Ma [McArthur *et al.*, 2001]. Fresh Indian Ocean MORB, presumably reflective of the composition of the mantle beneath the Cretaceous Tethys Ocean, has an $^{87}Sr/^{86}Sr$ of ~0.7031 [White and Klein, in press]. Rocks produced by reaction between Tethyan Ocean water and the Tethyan oceanic crust shouldl thus have $^{87}Sr/^{86}Sr$ between 0.7031 and 0.7074, depending on the degree of alteration. Most fresh samples in this study have $^{87}Sr/^{86}Sr$ values of 0.7031, consistent with unaltered MORB value. $^{87}Sr/^{86}Sr$ greater than MORB values are seen in rocks from upper gabbro section to the MTZ, indicative water - rock interaction throughout the oceanic crust.

However, OM7, OM8, OM8A and OM8C from the MTZ, OM49 from Moho, and OM45 from the upper gabbro have $^{87}Sr/^{86}Sr$ values higher than Cretaceous seawater, which indicates that these rocks have been altered by some process other than Cretaceous seawater-rock interaction. X-ray diffraction analysis (XRD) of OM8 and OM8C proved the two samples are composed of magnesite. The veins in OM45 effervesced under diluted HCl, suggesting they consist of calcite. Carbonate veins are not observed in samples OM7, OM8A and OM49. However, these three samples are highly fractured peridotites (Figure 15). Serpentine replacing olivine crystal is pervasive in the three samples. Apparent hydration and carbonation have affected these samples that have high $^{87}Sr/^{86}Sr$ values.

Leaching experiments on OM7, OM8A, OM45, OM49 gave interesting results (Table 10). There is no difference in $^{87}Sr/^{86}Sr$ (0.7084 ~ 0.7086) between the leachate and residue rock for peridotites OM7, OM8A and OM49. For OM 45, $^{87}Sr/^{86}Sr$ of

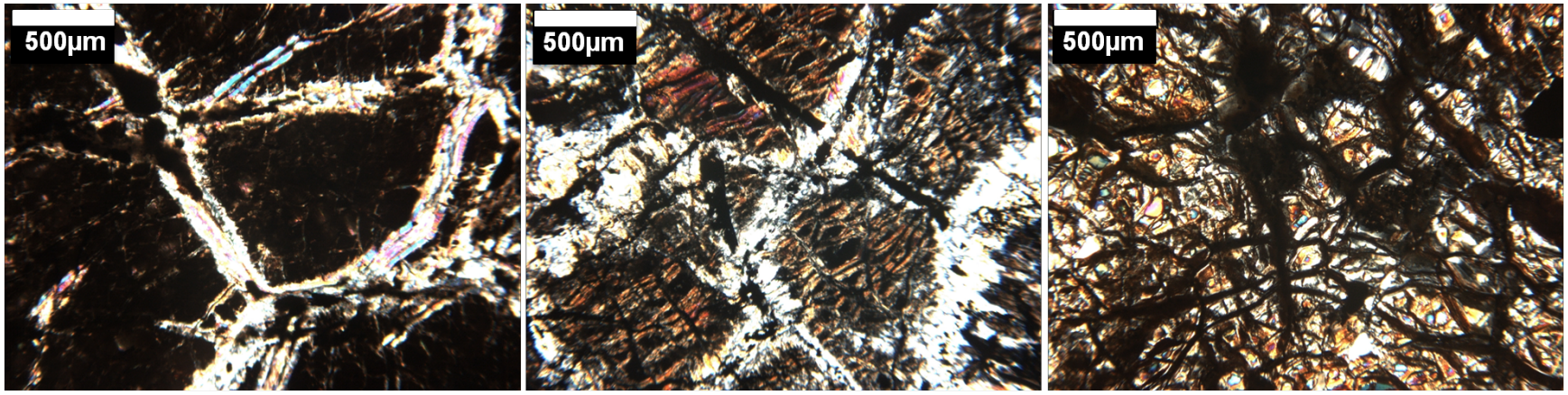

Figure 15. Thin section images of highly altered OM7, OM8A and OM49 under cross polarized light. Serpentinization is pervasive in the rocks.

the leachate is 0.7082 and that of the residue rock is 0.7070, suggesting that the whole rock $^{87}Sr/^{86}Sr$ of OM45 was largely overprinted because of the carbonates. Hydration of OM7, OM8A and OM49 was so extensive that the original isotopic composition is completely overprinted. The reason that peridotites have entirely overprinted $^{87}Sr/^{86}Sr$ ratios might be their low Sr concentrations. A small amount of Sr will disturb the Sr isotopic system of peridotite. OM45 that preserves some of the original rock information in the residue rock is from the upper gabbro section and has more Sr.

One possible source of carbonation and hydration is the precipitation of carbonate minerals in cracks when the Oman ophiolite was formed at spreading ridge. If the carbonates were Cretaceous precipitation, their $^{87}Sr/^{86}Sr$ should be similar to the seawater from which they precipitated. However, leaching experiments showed that the carbonates within the cracks also have $^{87}Sr/^{86}Sr$ greater than 0.7073, the Cretaceous seawater value. Thus, the leaching experiment results indicate the carbonates did not precipitate from Cretaceous seawater.

The carbonates might also have formed during obduction of the Oman ophiolite. Geochronology studies suggested that the obduction finished within one or two million years after formation of the Oman ophiolite. The seawater $^{87}Sr/^{86}Sr$ value shouldn't change very much within the one or two million years. As a result, high $^{87}Sr/^{86}Sr$ carbonation and hydration also could not have resulted by precipitating carbonates from seawater during the obduction.

Because of the fast obduction process, there is high chance that the hydration and carbonation of occurred after the obduction. In order to find out the precipitation age of the carbonates, geochronology study of carbonates is necessary. Mervine *et al.*, (2010) did ^{14}C dating of carbonate alteration of peridotite inthe Oman ophiolite. According to their work, carbonate veins that cut through peridotites are older than 50,000 years (the limit of ^{14}C dating), while carbonate veins on the peridotite weathering surface have ^{14}C age 29,000 ~ 44,000 years. The other type of carbonates, actively forming and fossil travertine, have ages between 5,000 ~ 24,000 years. Thus hydration and carbonation are on-going processes in Oman. Thus the $^{87}Sr/^{86}Sr$ greater than Creataceous seawater likely reflects relatively recent carbonation/hydration of the ophiolite. High $^{87}Sr/^{86}Sr$ could be derived from modern seawater (via the atmosphere and rain) or from sedimentary rocks in the area.

OM7 and OM8A were collected from an abandoned prehistoric copper mine. The sampling site has been through both a primary copper mineralization process and a secondary carbonation process. The high $^{87}Sr/^{86}Sr$ ratios of the two samples might be closely related to one or both of the processes. OM49 is from Wadi Al Abyad (Figure 16). The sample was collected near the water table level. Modern seawater has $^{87}Sr/^{86}Sr$ of 0.7092 [McArthur *et al.*, 2001]. The Oman mountains are close to the ocean, and the rainwater should have $^{87}Sr/^{86}Sr$ close to 0.7092. The high $^{87}Sr/^{86}Sr$ of OM49 might come from the long-term interaction with meteoric water. The stream that passes through Wadi Al Abyad might also have affected the

Figure 16. Field image of Wadi Al Abyad. OM49 was collected near the water table.

$^{87}Sr/^{86}Sr$ of OM49. All these assumptions for OM7, OM8A and OM49 suggest near surface alteration processes that affect the isotopic values of these samples.

CONCLUSIONS

The Oman ophiolite, one of the best-preserved ophiolite sequences, provides the ideal analogy of a mid-ocean ridge. Geochemical study of the Oman ophiolite can thus help to understand the modern hydrothermal circulation systems at spreading centers. As suggested by Gregory and Taylor (1981), hydrothermal alteration is pervasive in the Oman ophiolite: hydrothermal fluid can percolate through the depth of lower gabbro and locally penetrate into Moho Transition Zone. However, the circulation system is not a decoupled two-layer alteration system, as they suggested. Instead, high temperature alteration and low temperature alteration are alternately swiping down to lower gabbro section [Nicolas *et al.,* 2003; Bosch *et al*., 2004]. The fractures and veins in the oceanic lithosphere control the occurring of alterations. The development of orthopyroxene coronas between olivine and plagioclase proved the alteration temperature can reach 1000°C [Bosch *et al*., 2004]. As a result, the 350°C of black smokers is not the maximum alteration temperature in a hydrothermal circulation system. The temperature of fluids in hydrothermal vents observed on seafloor might be the result of seawater reaching critical point at the bottom of ocean. Fixation of CO_2 into ultramafic rocks after the obduction has changed the isotopic compositions of rocks, increasing the $^{87}Sr/^{86}Sr$ and $\delta^{18}O$ values, which should be considered when interpreting isotope ratios of ophiolites.

APPENDIX

Summarization of ratios plotted in Figure 13. Samples/OM34 have comparable ratios in Zr and Gd (bold), which are selected as immobile elements.

	OM9A/OM34	OM9B/OM34	OM31/OM34	OM33/OM34	OM35/OM34	OM37A/OM34	OM38/OM34	OM39/OM34
SiO_2	1.02	1.04	1.00	1.04	1.02	1.01	0.91	0.91
Al_2O_3	1.01	0.87	1.25	0.99	0.98	1.19	0.87	1.10
FeO	0.89	0.87	0.61	0.77	0.97	0.64	1.12	0.49
MnO	1.07	0.97	0.77	0.76	1.15	0.77	0.88	0.50
MgO	0.95	0.96	0.71	0.93	1.00	0.85	0.82	0.64
CaO	1.05	1.12	1.10	1.09	1.08	1.08	0.90	0.91
Na_2O	1.08	0.91	0.93	0.93	0.89	1.14	1.20	1.64
P_2O_5	1.13	1.27	1.03	1.24	1.09	1.07	0.86	1.22
Cr_2O_3	0.72	1.83	0.34	0.71	0.65	0.06	0.71	0.13
Cs	1.03	1.12	1.20	1.21	1.01	1.01	1.23	1.02
Rb	0.99	1.21	1.76	1.28	1.01	0.99	1.10	1.01
Ba	1.33	1.51	2.07	1.08	1.18	0.87	2.75	1.44
Ce	1.11	1.28	1.07	1.12	1.09	1.00	1.15	1.02
Pr	1.39	1.88	1.26	1.47	1.35	0.85	1.58	1.35
Sr	1.01	0.80	1.60	1.17	0.94	1.68	1.20	1.67
Nd	1.25	1.62	1.17	1.40	1.24	0.90	1.42	1.16
Zr	**1.05**	**1.21**	**1.03**	**1.07**	**1.02**	**1.00**	**1.09**	**0.91**
Hf	1.15	1.40	1.10	1.19	1.16	0.95	1.29	1.02
Sm	1.29	1.82	1.17	1.57	1.30	0.81	1.52	1.20
Eu	1.20	1.41	1.03	1.24	1.19	0.87	1.29	1.13
Gd	**1.09**	**1.27**	**1.04**	**1.17**	**1.08**	**0.98**	**1.15**	**0.96**
Tb	1.14	1.41	1.07	1.29	1.13	0.94	1.24	1.02
Dy	1.27	1.79	1.14	1.57	1.28	0.82	1.48	1.16
Ho	1.26	1.80	1.13	1.58	1.28	0.82	1.49	1.17
Y	1.10	1.55	0.99	1.37	1.05	0.75	1.20	0.90
Er	1.34	2.02	1.16	1.74	1.34	0.76	1.63	1.25
Tm	1.44	2.39	1.23	2.04	1.47	0.64	1.87	1.39
Yb	1.34	2.07	1.17	1.81	1.37	0.75	1.67	1.27
Lu	1.57	2.73	1.27	2.34	1.57	0.54	2.09	1.52
Ni	0.62	0.69	0.44	0.48	0.58	0.59	0.30	0.46

REFERENCES

Ague, J.J., 1994, Mass transfer during Barrovian metamorphism of pelites, south-central Connecticut; I, Evidence for changes in composition and volume: American Journal of Science, v. 294, no. 8, p. 989-1057.

Ague, J.J., and van Haren, J.L.M., 1996, Assessing metasomatic mass and volume changes using the bootstrap, with application to deep crustal hydrothermal alteration of marble: Economic Geology, v. 91, no. 7, p. 1169 -1182.

Alabaster, T., Pearce, J.A., and Malpas, J., 1982, The volcanic stratigraphy and petrogenesis of the Oman ophiolite complex: Contributions to Mineralogy and Petrology, v. 81, p. 168-183.

Aubouin, J., and Ndojaj, I. Regard sur la géologie de l'Albanie et sa place dans la géologie des Dinarides: Bulletin de la Société Géologique de France, v. 7, p. 593-625.

Benoit, M., Polvé, M., and Ceuleneer, G., 1996, Trace element and isotopic characterization of mafic cumulates in a fossil mantle diapir (Oman ophiolite): Chemical Geology, v. 134, no. 1-3, p. 199-214.

Benson, W.N., 1920, Tectonic conditions accompanying intrusion of basic and ultra-basic igneous rocks: Geological Society of America Bulletin, v. 31, no. 1, p. 144-148.

Bezzi, A., and Piccardo, G.B., 1971, Structural features of the ligurian ophiolites: Petrologic evidence for the "oceanic" floor of the northern Apennines Geosyncline: a contribution to the problem of the Alpine type gabbro-peridotite associations: Mem. Soc. Geol. It., v. 10, p. 53-63.

Bosch, D., Jamais, M., Boudier, F., Nicolas, A., Dautria, J.-M., and Agrinier, P., 2004, Deep and high-temperature hydrothermal circulation in the Oman ophiolite—petrological and isotopic evidence: Journal of Petrology, v. 45, no. 6, p. 1181 -1208.

Boudier, F., Ceuleneer, G., and Nicolas, A., 1988, Shear zones, thrusts and related

magmatism in the Oman ophiolite: Initiation of thrusting on an oceanic ridge: Tectonophysics, v. 151, no. 1-4, p. 275-275-296.

Bowen, N.L., 1927, The origin of ultrabasic and related rocks: American Journal of Science, v. s5-14, no. 80, p. 89-108.

Brimhall, G., and Dietrich, W., 1987, Constitutive mass balance relations between chemical composition, volume, density, porosity, and strain in metasomatic hydrochemical systems: Results on weathering and pedogenesis: Geochimica et Cosmochimica Acta, v. 51, p. 567-587.

Brongniart, A., 1813, Essai d'une classification minéralogique des roches mélangées: Bossande, Paris.

Brongniart, A., 1821, Sur le gisement, ou position relative des ophiolites, euphotides, jaspes, etc., dans quelques parties des Apennins: De l'Imprimerie de Madame Huzard (née Vallat la Chapelle) rue de l'Éperon-Saint-André-des Arts no. 7., Paris.

Brunn, J., 1956, Contribution à l'étude géologique du Pinde septentrional et d'une partie de la Macédoine occidentale. [With a map.].: Athènes.

Brunn, J., 1961, Les sutures ophiolitiques: contribution a I'études des relations entre phénomene magmatique et orogénique: Revue de Géographie Physique et Géologie Dynamique, v. 4, p. 89-96,181-202.

Brunn, J., 1960, Mise en place et différenciation de l'association pluto-volcanique du cortège ophiololitique: Revue de Géographie Physique et Géologie Dynamique, v. 3, p. 115-132.

Cathles, L.M., 1983, An analysis of the hydrothermal system responsible for massive sulfide deposition in the Hokuroku Basin of Japan: Economic Geology Monograph, v. 5, p. 439-487.

Cheatham, M.M., Sangrey, W.F., and White, W.M., 1993, Sources of error in external calibration ICP-MS analysis of geological samples and an improved non-linear drift correction procedure: Spectrochimica Acta Part B: Atomic Spectroscopy, v. 48, p. 487-506.

Coleman, R.G., 1981, Tectonic Setting for Ophiolite Obduction in Oman: Journal of Geophysical Research, v. 86, no. B4, p. 2497–2508.

Cox, K.G., Bell, J.D., and Pankhurst, R.J., 1979, The interpretation of igneous rocks: G. Allen & Unwin, London, Boston.

Craig, H., 1961, Standard for reporting concentrations of Deuterium and oxygen-18 in natural waters: Science, v. 133, no. 3467, p. 1833 -1834.

Dilek, Y., 2003, Ophiolite concept and its evolution: Geological Society of America Special Papers, v. 373, p. 1 -16.

Dubertret, L., 1953, Géologie des roches vertes du nord-ouest de la Syrie et du Hatay (Turquie): Notes et Mem. sur le Moyen-Orient, v. 4.

Ewing, J., and Ewing, M., 1959, Seismic-refraction measurements in the Atlantic Ocean basins, in the Mediterranean Sea, on the Mid-Atlantic Ridge, and in the Norwegian Sea: Geological Society of America Bulletin, v. 70, no. 3, p. 291-318.

Foumier, R.O. The transition from hydrostatic to greater than hydrostatic fluid pressure in presently active continental hydrothermal systems in crystalline rock: Geophysical Research Letters, v. 18, no. 5, p. 955–958.

Gass, I.G., 1968, Is the Troodos Massif of Cyprus a Fragment of Mesozoic Ocean Floor?: Nature, v. 220, no. 5162, p. 39-42.

Ghent, E.D., and Stout, M.Z. Metamorphism at the base of the Samail Ophiolite, southeastern Oman Mountains: Journal of Geophysical Research, v. 86, no. B4, p. 2557-2571.

Glennie, K.W., 1974, Geology of the Oman Mountains: Verh. K. Ned. Geol. Mijnbouwkd. Genoot., v. 31.

Glennie, K.W., Boeuf, M.G.A., Clarke, M.W.H., Moody-Stuart, M., Pilaar, W.F.H., and Reinhardt, B.M., 1973, Late Cretaceous nappes in Oman Mountains and their geologic evolution: AAPG Bulletin, v. 57, no. 1, p. 5-27.

Grant, J.A., 1986, The isocon diagram; a simple solution to Gresens' equation for metasomatic alteration: Economic Geology and the Bulletin of the Society of Economic Geologists, v. 81, no. 8, p. 1976-1982.

Gray, D.R., Gregory, R.T., and Miller, J.M., 2000, A new structural profile along the Muscat-Ibra transect, Oman: Implications for emplacement of the Samail Ophiolite: Geological Society of America Special Papers, v. 349, p. 513 -523.

Gregory, R.T., and Jr, H.P.T. An oxygen isotope profile in a section of Cretaceous oceanic crust, Samail Ophiolite, Oman: evidence for $\delta^{18}O$ buffering of the oceans by deep (>5 km) seawater-hydrothermal circulation at mid-ocean ridges: Journal of Geophysical Research, v. 86, no. B4, p. 2737-2755.

Gresens, R.L., 1967, Composition-volume relationships of metasomatism: Chemical Geology, v. 2, no. 0, p. 47-65.

Hacker, B.R., 1994, Rapid emplacement of young oceanic lithosphere: argon geochronology of the Oman Ophiolite: Science, v. 265, no. 5178, p. 1563 -1565.

Hacker, B.R., Mosenfelder, J.L., and Gnos, E., 1996, Rapid emplacement of the Oman ophiolite: Thermal and geochronologic constraints: Tectonics, v. 15, no. 6, p. PP. 1230-1247.

Hawkins, J.W., and Melchior, J.T. Petrology of Mariana Trough and Lau Basin basalts: Journal of Geophysical Research, v. 90, no. B13, p. 11,431-11,468.

Hey, R.N., Deffeyes, K.S., Johnson, G.L., and Lowrie, A., 1972, The Galapagos Triple Junction and plate motions in the East Pacific: Nature, v. 237, no. 5349, p. 20-22.

Ingebritsen, S.E., and Hayba, D.O., 1994, Fluid flow and heat transport near the critical point of H_2O: Geophysical Research Letters, v. 21, no. 20, p. 2199-2202.

Karson, J.A., 2002, Geologic structure of the uppermost oceanic crust created at fast- to intermediate-rate spreading centers: Annual Review of Earth and Planetary Sciences, v. 30, p. 347-384.

Kawahata, H., Nohara, M., Ishizuka, H., Hasebe, S., and Chiba, H., 2001, Sr isotope geochemistry and hydrothermal alteration of the Oman ophiolite: Journal of Geophysical Research, v. 106, no. B6, p. 11,083-11,099.

Kay, S.M., Maksaev, V., Moscoso, R., Mpodozis, C., and Nasi, C., 1987, Probing the evolving Andean lithosphere: mid-late tertiary magmatism in Chile (29°-30°30'S) over the modern zone of subhorizontal subduction: Journal of Geophysical Research, v. 92, p. 6173-6190.

Kelemen, P.B., and Matter, J., 2008, In situ carbonation of peridotite for CO_2 storage: Proceedings of the National Academy of Sciences, v. 105, no. 45, p. 17295 - 17300.

Koepke, J., Feig, S.T., Snow, J., and Freise, M., 2004, Petrogenesis of oceanic plagiogranites by partial melting of gabbros: an experimental study: Contributions to Mineralogy and Petrology, v. 146, p. 414-432.

Lackner, K., 1995, Carbon dioxide disposal in carbonate minerals: Energy, v. 20, no. 11, p. 1153-1153-1170.

Lanphere, M.A., Coleman, R.G., and Hopson, C.A., 1981, Sr isotopic tracer study of the Samail Ophiolite, Oman: Journal of Geophysical Research, v. 86, no. B4, p. 2709-2720.

Liou, J.G., Kuniyoshi, S., and Ito, K., 1974, Experimental studies of the phase relations between greenschist and amphibolite in a basaltic system: Am J Sci, v. 274, no. 6, p. 613-632.

Lippard, S.J., Shelton, A.W., and Gass, I.G., 1986, The ophiolite of northern Oman: Published for the Geological Society by Blackwell Scientific Publications.

Lister, C.R.B., 1974, On the penetration of water into hot rock: Geophysical Journal of the Royal Astronomical Society, v. 39, no. 3, p. 465-509.

Manning, C.E., MacLeod, C.J., and Weston, P.E., 2000, Lower-crustal cracking front at fast-spreading ridges: Evidence from the East Pacific Rise and the Oman Ophiolite: Geological Society of America Special Papers, v. 349, p. 261 -272.

Manning, C.E., Weston, P.E., and Mahon, K.I., 1996, Rapid high-temperature metamorphism of East Pacific Rise gabbros from Hess Deep: Earth and Planetary Science Letters, v. 144, p. 123-132.

McArthur, J.M., Howarth, R.J., and Bailey, T.R., 2001, Strontium Isotope Stratigraphy: LOWESS Version 3: Best Fit to the Marine Sr-Isotope Curve for 0-509 Ma and Accompanying Look-up Table for Deriving Numerical Age: Journal of Geology, v. 109, p. 155-170.

McCulloch, M.T., Gregory, R.T., Wasserburg, G.J., and Jr, H.P.T., 1981, Sm-Nd, Rb-Sr, and $^{18}O/^{16}O$ isotopic systematics in an oceanic crustal section: evidence from the Samail Ophiolite: Journal of Geophysical Research, v. 86, no. B4, p. 2721-2735.

Mervine, E.M., Kelemen, P.B., Sims, K.W., Humphris, S.E., Jenkins, W.J., and Roberts, M., 2010, 14C dating of carbonate alteration of peridotite in the Samail Ophiolite, Oman: American Geophysical Union, Fall Meeting, abstract #GC31B-0867 2010,.

Muehlenbachs, K., and Clayton, R.N., 1976, Oxygen isotope composition of the oceanic crust and its bearing on seawater: Journal of Geophysical Research, v. 81, no. 23, p. 4365-4369.

Muehlenbachs, K., Furnes, H., Fonneland, H.C., and Hellevang, B., 2003, Ophiolites as faithful records of the oxygen isotope ratio of ancient seawater: the Solund-Stavfjord Ophiolite Complex as a Late Ordovician example: Geological Society, London, Special Publications, v. 218, no. 1, p. 401 -414.

Nicolas, A., 1986, Structure and petrology of peridotites: Clues to their geodynamic environment: Reviews of Geophysics, v. 24, no. 4, p. 875-895.

Nicolas, A., 1989, Structures of ophiolites and dynamics of oceanic lithosphere: Springer.

Nicolas, A., Boudier, F., Ildefonse, B., and Ball, E., 2000, Accretion of Oman and United Arab Emirates ophiolite - Discussion of a new structural map: Marine Geophysical Researches, v. 21, p. 147-180.

Nicolas, A., and Boudier. F., 2000, Large mantle upwellings and related variations in crustal thickness in the Oman ophiolite: Geological Society of America Special Papers, v. 349, p. 67-73.

Nicolas, A., Ceuleneer, G., Boudier, F., and Misseri, M., 1988, Structural mapping in the Oman ophiolites: Mantle diapirism along an oceanic ridge: Tectonophysics, v. 151, p. 27-56.

Nicolas, A., Mainprice, D., and Boudier, F., 2003, High-temperature seawater circulation throughout crust of oceanic ridges: A model derived from the Oman ophiolites: Journal of Geophysical Research, v. 108.

O'Neil, J.R., 1969, Oxygen isotope fractionation in divalent metal carbonates: The Journal of Chemical Physics, v. 51, p. 5547.

O'Neil, J.R., and Taylor, H.P., 1967, The oxygen isotope and cation exchange chemistry of feldspars: American Mineralogist, v. 52, p. 1414-1437.

Pallister, J.S., and Hopson, C.A. Samail Ophiolite plutonic suite: Field relations, phase variation, cryptic variation and layering, and a model of a spreading ridge magma chamber: Journal of Geophysical Research, v. 86, no. B4, p. 2593-2644.

Pearce, J.A., Alabaster, T., Shelton, A.W., and Searle, M.P., 1981, The Oman ophiolite as a Cretaceous arc-basin complex: Evidence and implications: Philosophical Transactions of the Royal Society of London. Series A, Mathematical and Physical Sciences, v. 300, no. 1454, p. 299-317.

Pearce, J.A., Lippard, S.J., and Roberts, S., 1984, Characteristics and tectonic significance of supra-subduction zone ophiolites: Geological Society, London, Special Publications, v. 16, no. 1, p. 77 -94.

Philpotts, A.R., and Ague, J.J., 2009, Principles of igneous and metamorphic petrology: Cambridge University Press.

Robertson, A., 2004, Development of concepts concerning the genesis and emplacement of Tethyan ophiolites in the Eastern Mediterranean and Oman regions: Earth-Science Reviews, v. 66, no. 3-4, p. 331-387.

Searle, M.P., and Cox, J., 2002, Subduction zone metamorphism during formation and emplacement of the Semail ophiolite in the Oman Mountains: Geological Magazine, v. 139, no. 3, p. 241-255.

Searle, M., and Cox, J., 1999, Tectonic setting, origin, and obduction of the Oman ophiolite: Geological Society of America Bulletin, v. 111, no. 1, p. 104 -122.

Searle, M.P., and Malpas, J., 1982, Petrochemistry and origin of sub-ophiolitic metamorphic and related rocks in the Oman Mountains: Journal of the Geological Society, v. 139, no. 3, p. 235-248.

Searle, M.P., and Malpas, J., 1980, The structure and metamorphismof rocks beneath the Semail Ophiolite ofOman and their significance in ophiolite obduction: Transactions Royal Society, Edinburgh, Earth Sciences, v. 71, p. 247-262.

Searle, M.P., and Stevens, R.K., 1984, Obduction processes in ancient, modern and future ophiolites: Geological Society, London, Special Publications, v. 13, no. 1, p. 303 -319.

Seifritz, W., 1990, CO2 disposal by means of silicates: Nature, v. 345, no. 6275, p. 486.

Sinton, J.M., and Fryer, P. Mariana Trough lavas from 18°N: implications for the origin of back arc basin basalts: Journal of Geophysical Research, v. 92, no. B12, p. 802.

Spear, F.S., 1981, An experimental study of hornblende stability and compositional variability in amphibolite: American Journal of Science, v. 281, no. 6, p. 697-734.

Stein, C.A., and Stein, S., 1994, Constraints on hydrothermal heat flux through the oceanic lithosphere from global heat flow: Journal of Geophysical Research, v. 99, no. B2, p. 3081–3095.

Steinmann, G., Bernoulli, D., and Friedman, G.M., 2003, Die ophiolitischen Zonen in den mediterranean Kettengebirgen: Geological Society of America Special Papers, v. 373, p. 77 -91.

Tarney, J., Saunders, A.D., Mattey, D.P., Wood, D.A., Marsh, N.G., Roberts, D., and Stegena, L., 1981, Geochemical aspects of back-arc spreading in the Scotia Sea and Western Pacific: Philosophical Transactions of the Royal Society of London. Series A, Mathematical and Physical Sciences, v. 300, no. 1454, p. 263 -285.

Taylor, H.P., 1974, The application of oxygen and hydrogen isotope studies to problems of hydrothermal alteration and ore deposition: Economic Geology, v. 69, no. 6, p. 843-883.

Tilton, G.R., Hopson, C.A., and Wright, J.E., 1981, Uranium-Lead isotopic ages of the Samail ophiolite, Oman, with applications to Tethyan Ocean ridge tectonics: Journal of Geophysical Research, v. 86, no. B4, p. 2763-2775.

Veizer, J., Ala, D., Azmy, K., Bruckschen, P., Buhl, D., Bruhn, F., Carden, G.A.F., Diener, A., Ebneth, S., Godderis, Y., Jasper, T., Korte, C., Pawellek, F., Podlaha, O.G., et al., 1999, $^{87}Sr/^{86}Sr$, $\delta^{13}C$ and $\delta^{18}O$ evolution of Phanerozoic seawater: Chemical Geology, v. 161, no. 1-3, p. 59-88.

Wenner, D.B., and Taylor, H.P., 1971, Temperatures of serpentinization of ultramafic rocks based on O18/O16 fractionation between coexisting serpentine and magnetite: Contributions to Mineralogy and Petrology, v. 32, p. 165-185.

Wenner, D.B., and Taylor Jr., H.P., 1974, D/H and O^{18}/O^{16} studies of serpentinization of ultramaflc rocks: Geochimica et Cosmochimica Acta, v. 38, no. 8, p. 1255-1286.

White, W.M., and Duncan, R.A., 1996, Geochemistry and geochronology of the Society Islands; new evidence for deep mantle recycling: Geophysical Monograph, v. 95, p. 183-206.

White, W.M., and Klein, E., 2011, The Volcanic Oceanic Crust, in press